MKS and NPHP modules cooperate to establish basal body/transition zone membrane associations and ciliary gate function during ciliogenesis

Corey L. Williams,[1] Chunmei Li,[2] Katarzyna Kida,[3] Peter N. Inglis,[2] Swetha Mohan,[2] Lucie Semenec,[2] Nathan J. Bialas,[2] Rachel M. Stupay,[1] Nansheng Chen,[2] Oliver E. Blacque,[3] Bradley K. Yoder,[1] and Michel R. Leroux[2]

[1]Department of Cell Biology, University of Alabama at Birmingham Medical Center, Birmingham, AL 35294
[2]Department of Molecular Biology and Biochemistry, Simon Fraser University, Burnaby, British Columbia V5A 1S6, Canada
[3]School of Biomolecular and Biomedical Science, UCD Conway Institute, University College Dublin, Belfield, Dublin 4, Ireland

Meckel-Gruber syndrome (MKS), nephronophthisis (NPHP), and related ciliopathies present with overlapping phenotypes and display considerable allelism between at least twelve different genes of largely unexplained function. We demonstrate that the conserved *C. elegans* B9 domain (MKS-1, MKSR-1, and MKSR-2), MKS-3/TMEM67, MKS-5/RPGRIP1L, MKS-6/CC2D2A, NPHP-1, and NPHP-4 proteins exhibit essential, collective functions at the transition zone (TZ), an underappreciated region at the base of all cilia characterized by Y-shaped assemblages that link axoneme microtubules to surrounding membrane. These TZ proteins functionally interact as members of two distinct modules, which together contribute to an early ciliogenic event. Specifically, MKS/MKSR/NPHP proteins establish basal body/TZ membrane attachments before or coinciding with intraflagellar transport–dependent axoneme extension and subsequently restrict accumulation of nonciliary components within the ciliary compartment. Together, our findings uncover a unified role for eight TZ-localized proteins in basal body anchoring and establishing a ciliary gate during ciliogenesis, and suggest that disrupting ciliary gate function contributes to phenotypic features of the MKS/NPHP disease spectrum.

Introduction

Primary cilia protrude from most mammalian cells and modulate sensory processes, including chemo-, mechano-, and photoreception (Fliegauf et al., 2007). Cilia regulate various signaling pathways during embryonic development and are needed for normal postnatal tissue homeostasis (Gerdes et al., 2009). Mutations disrupting ciliary functions cause human disorders (ciliopathies) that collectively affect nearly all tissues/organs (Sharma et al., 2008). A nonexhaustive list of ciliopathies includes Meckel-Gruber syndrome (MKS), nephronophthisis (NPHP), Bardet-Biedl syndrome (BBS), Joubert syndrome (JBTS), Senior-Løken syndrome (SLSN), Leber congenital amaurosis (LCA), polycystic kidney disease (PKD), and oral-facial-digital syndrome (OFD). These disorders present with variable but overlapping clinical phenotypes that encompass polycystic kidneys, liver fibrosis, skeletal anomalies, sensory impairment, and brain/nervous system deformities (Fliegauf et al., 2007).

At least 35 loci have been identified in ciliopathy patients, some of which contribute to multiple seemingly distinct syndromes (Baker and Beales, 2009). Many of these genes encode proteins that localize to the basal body (BB)—a centriolar structure universally required for extending the microtubule-based ciliary axoneme—or to an adjacent domain, termed "transition zone" (TZ) in most cilia, or "connecting cilium" in photoreceptors (Horst et al., 1990; see schematic of BB-TZ-cilia structures in Fig. 1 A and relevant disease proteins in Table S1 A). Within the BB-TZ region are subdomains that include transitional fibers (TFs) and Y-links. TFs form a pinwheel-like structure, of unknown

C.L. Williams, C. Li, and K. Kida contributed equally to this paper.

Correspondence to Michel R. Leroux: leroux@sfu.ca; Bradley K. Yoder: byoder@uab.edu; or Oliver E. Blacque: oliver.blacque@ucd.ie

Abbreviations used in this paper: BB, basal body; BBS, Bardet-Biedl syndrome; IFT, intraflagellar transport; MKS, Meckel-Gruber syndrome; NPHP, nephronophthisis; TEM, transmission electron microscopy; TF, transitional fiber; TZ, transition zone.

The Rockefeller University Press $30.00
J. Cell Biol. Vol. 192 No. 6 1023–1041
www.jcb.org/cgi/doi/10.1083/jcb.201012116

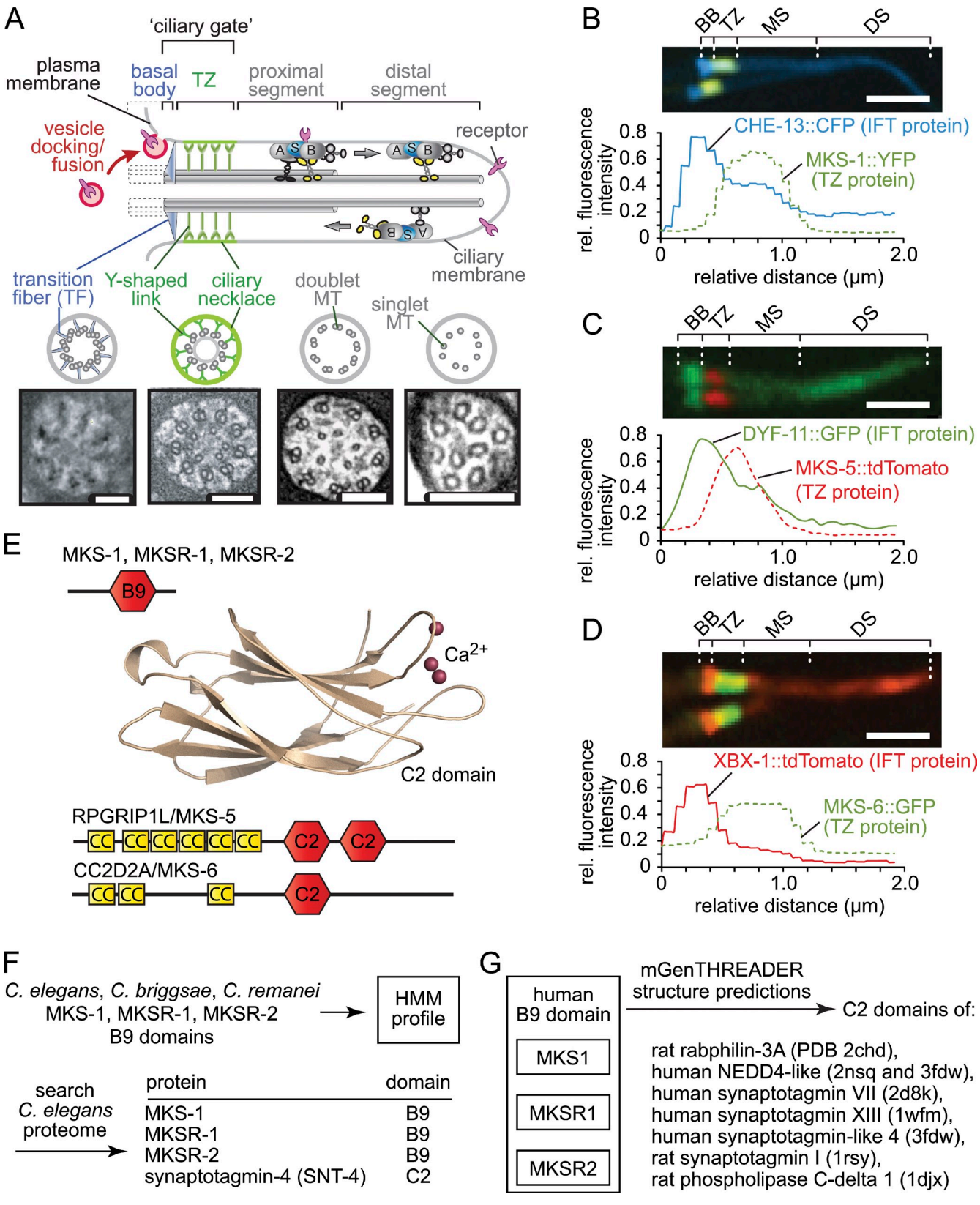

Figure 1. ***C. elegans* B9 and C2 domain ciliopathy proteins are found at the transition zone, adjacent to the basal body/transition fiber region.** (A) Schematic of a prototypical basal body (BB)/transition zone (TZ)/cilium, highlighting the microtubule (MT) backbone of the organelle, the docking of vesicles at the base of a "ciliary gate," and its intraflagellar transport (IFT) trafficking machinery. In *C. elegans*, the BB lacks discernable MTs (shown dashed) and consists mainly of transition fibers (TFs). The TZ is demarcated by Y-links spanning the axoneme to the membrane and likely organizes the "ciliary necklace" on the ciliary membrane. The TFs and TZ are proposed to form a gate that restricts entry of vesicles and potentially also nonciliary proteins. TEM cross sections from *C. elegans* show relevant substructures (TFs, TZ, middle and distal cilia segments; Bars, 100 nm). IFT particles carry cargo from the BB into cilia; kinesins transport two multi-protein complexes (IFT subcomplexes A and B) and a BBS protein complex (S) along with cargo, and dynein recycles

protein composition, that links the BB to the proximal ciliary membrane. The Y-links of the TZ connect—via high-affinity linkages—axonemal microtubules to the membrane at the ciliary necklace, a proteinaceous decoration of the TZ membrane (Muresan and Besharse, 1994). Together, the TFs and TZ are proposed to form a gate (Rosenbaum and Witman, 2002; Satir and Christensen, 2007) that excludes vesicles from cilia, prevents unwanted diffusion of membrane proteins into cilia, and selectively regulates protein ciliary entry and exit (Fig. 1 A).

Axoneme elongation is thought to initiate when the mother centriole docks with a membrane either at the cell surface or a ciliary vesicle in the cytosol (see Fig. 10 D; Sorokin, 1962). Full extension of the axoneme then relies on an intraflagellar transport (IFT) machinery that uses kinesin and dynein motors and associated subcomplexes (IFT-A, IFT-B, and BBSome) to traffic ciliary cargo from TFs to the cilium tip and back (Fig. 1 A; Silverman and Leroux, 2009). In contrast to the extensive characterization of IFT-mediated axoneme extension, the components and mechanism involved in BB/TZ membrane association and establishment of the ciliary gate remain virtually unknown. Based on knockdown studies in mammalian cells, the ciliopathy proteins MKS1 and MKS3 have been implicated in BB migration/docking and thus ciliogenesis (Dawe et al., 2007). However, these defects are absent from rodent *Mks1* or *Mks3* mutants (Tammachote et al., 2009); thus, the role of these and most other BB/TZ-associated ciliopathy proteins remains unclear. Recently, the ciliopathy protein CEP290 was localized to TZ Y-links, and its disruption in *Chlamydomonas* altered the ciliary composition of IFT components and other proteins (Craige et al., 2010); *Caenorhabditis elegans* NPHP-1 and NPHP-4 have also been proposed to act in ciliary gating (Jauregui et al., 2008). Whether additional TZ or IFT proteins are similarly involved in regulating ciliary gating, and the mechanism by which they perform these functions, is not known.

Here, we used *C. elegans* to elucidate the functions of eight conserved proteins, six of which are MKS/NPHP associated. We find that MKS-5/RPGRIP1L interacts with two distinct TZ functional modules, MKS/MKSR and NPHP, consisting of MKS-1/MKSR-1/MKSR-2/MKS-3/MKS-6 and NPHP-1/NPHP-4 proteins, respectively. Functional interactions between different MKS module components and the NPHP module are essential for an IFT-independent early stage of ciliogenesis, namely docking/anchoring of the BB/TZ to the membrane. Moreover, the two modules restrict inappropriate accumulation of membrane-associated proteins inside cilia. Our findings help to comprehensively define an interaction network of ciliopathy-associated proteins and allow us to propose for the first time a unified model for the function of diverse MKS/NPHP proteins, in which the MKS and NPHP modules altogether enable associations between microtubules and the ciliary membrane; this ciliogenic event coincides with construction of the ciliary gate that establishes the specialized compartment.

Results

MKS/MKSR and NPHP proteins localize specifically to the ciliary TZ

To gain insights into MKS/MKSR/NPHP protein functions, we first defined their respective subcellular localization in *C. elegans* sensory neurons. Using fluorescently tagged proteins, we detect MKS/MKSR/NPHP proteins in a region corresponding to the TZ (adjacent to where IFT proteins concentrate at the TFs/BB). This is evident for MKS-1, MKS-1 related-1 (MKSR-1)/B9D1, MKS-1 related-2 (MKSR-2)/B9D2, MKS-3/meckelin, NPHP-1, and NPHP-4 (Winkelbauer et al., 2005; Williams et al., 2008, 2010; Bialas et al., 2009), as well as MKS-5/RPGRIP1L and MKS-6/CC2D2A, previously uncharacterized in *C. elegans* (Fig. 1, B–D; Fig. 2). By transmission electron microscopy (TEM), the ∼0.8-µm long TZ region containing Y-links is distal to the TFs, which sit at the ciliary base just inside the dendritic tip (Fig. 1 A; Perkins et al., 1986). These data suggest that the TZ represents a common site of dysfunction in MKS/NPHP ciliopathy patients; however, the functions of MKS/MKSR/NPHP proteins at the TZ remain undetermined. Notably, based on Hidden Markov Model profiling and structure/fold predictions, several TZ proteins (MKS-1, MKSR-1, MKSR-2, MKS-5, and MKS-6) share a related C2/B9 motif (Fig. 1, E–G; Table S1 C). This motif is predicted to bind Ca^{2+}/lipids and participate—similar to synaptotagmin—in membrane/vesicle trafficking and fusion (Nalefski and Falke, 1996). The presence of this motif in multiple-ciliopathy TZ proteins raises the possibility that they perform a shared function at the TZ.

Functional interactions between NPHP proteins and MKS-5 or MKS-6 are required for ciliogenesis

To examine potential ciliary roles of the uncharacterized C2 domain–containing MKS-5 and MKS-6 proteins, we first analyzed *mks-5* and *mks-6* mutants (Fig. 3 A). Similar to mutations disrupting B9 domain genes (*mks-1*, *mksr-1*, and *mksr-2*; Williams et al., 2008; Bialas et al., 2009), *mks-6(gk674)* mutants have no overt cilia or IFT defects, based on: (1) normal uptake of

components back to the BB. (B) MKS-1::YFP localization to the TZ in relation to the CHE-13 IFT protein, which concentrates at BB/TFs and is present along the axoneme. Two phasmid (tail neuron) cilia are shown, as in C and D; all tagged proteins are expressed under endogenous promoters unless specified otherwise; MS, middle segment; DS, distal segment. Bar, 2 µm. (C and D) Similar to MKS-1, MKS-5::tdTomato and MKS-6::GFP (both *osm-5* promoter driven) localize to the TZ, which largely does not overlap with the peak intensities of tagged IFT proteins (DYF-11 and XBX-1, respectively) at the adjacent BB/TFs. Bars, 2 µm. (E) B9 domains of MKS-1, MKSR-1, and MKSR-2 may be structurally related to C2 domains of RGRIP1L/MKS-5 and CC2D2A/MKS-6 (see F and G). A representative structure of synaptotagmin I C2 domain (PDB code 1byn), with bound Ca^{2+}, is shown. (F) A Hidden Markov Model profile was created using B9 domains from *C. elegans*, *C. briggsae*, and *C. remanei* to search the *C. elegans* proteome for related domains in evolutionarily conserved proteins. Only four are retrieved: the B9 input proteins and a C2 domain protein, synaptotagmin-4 (SNT-4). (G) The top hits from the structure prediction algorithm GenTHREADER reveal that all three human B9 domains can be modeled onto known C2 domain NMR/crystal structures from different proteins (synaptotagmins, E3 ubiquitin-protein ligase NEDD4-like, phospholipase C-delta1, and rabphilin-3A; PDB codes in parentheses).

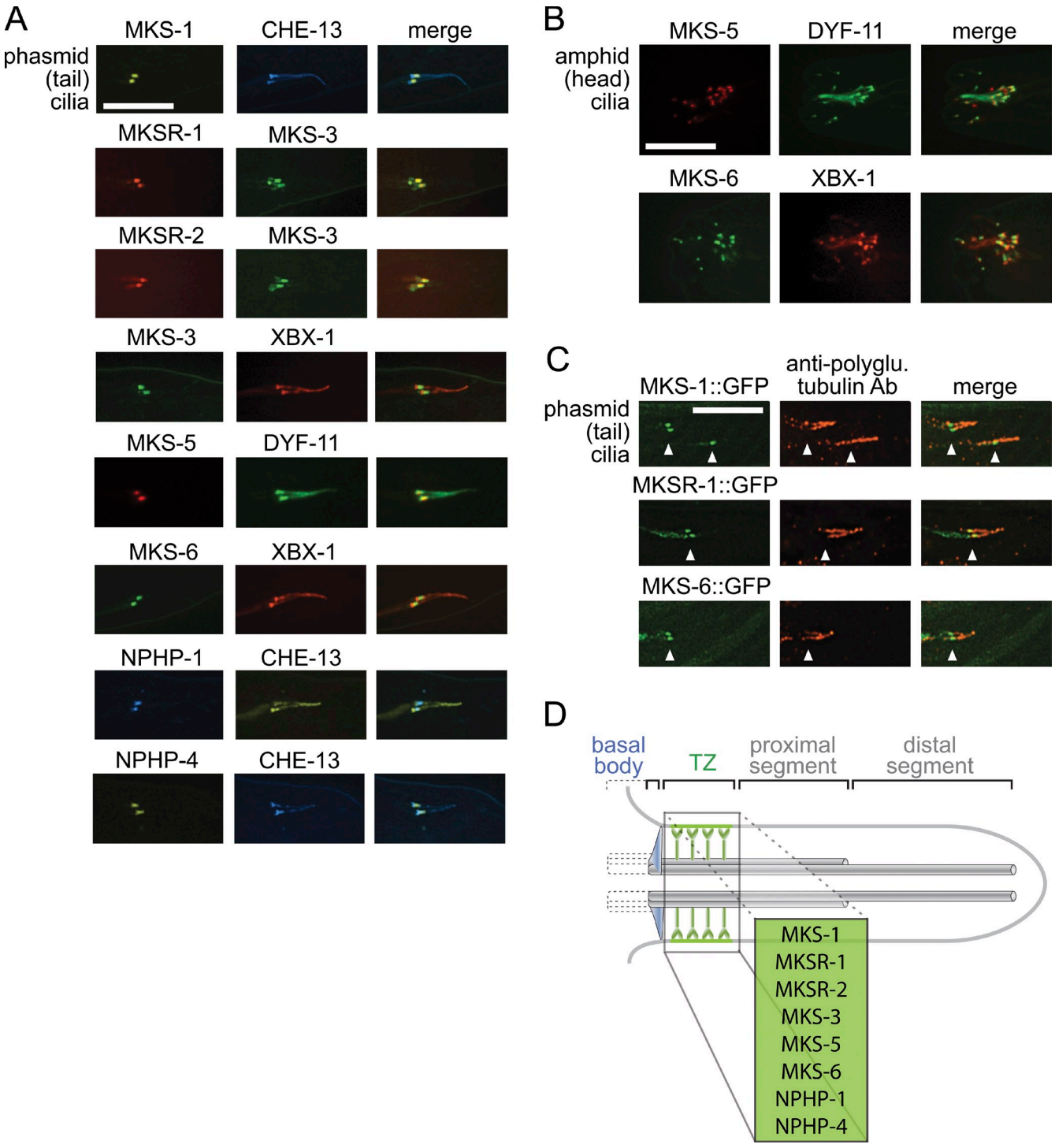

Figure 2. **MKS/MKSR and NPHP proteins localize at the ciliary TZ.** (A) Fluorophore-tagged MKS/MKSR and NPHP proteins localize at the TZ in tail cilia. Each TZ protein signal is overlaid with IFT or other TZ protein signal, as indicated. Bar, 10 µm. (B) MKS-5::tdTomato and MKS-6::GFP localize at the TZ in head cilia. MKS-5 and MKS-6 are overlaid with IFT proteins DYF-11::GFP and XBX-1::tdTomato, respectively. Bar, 10 µm. (C) GFP-tagged MKS-1, MKSR-1, and MKS-6 localize at the base of ciliary axonemes (consistent with the TZ), which are marked by staining with an antibody against polyglutamylated tubulin. Bar, 10 µm. (D) Schematic of MKS/MKSR/NPHP protein localization at the TZ.

hydrophobic fluorescent dye (DiI), indicating cilia are present and environmentally exposed (Fig. 3, B and D); (2) normal cilia length, observed by visualizing cilia with GFP-tagged IFT proteins (Fig. 4, B and C; Fig. 5, A, A′, B, and B′); and finally, (3) normal IFT rates, based on in vivo time-lapse microscopy (Table S1 D). TEM analysis verifies the absence of gross cilia ultrastructure anomalies in *mks-6(gk674)* mutants, except for occasional loss of axoneme distal segments (Fig. 6). *mks-6(gk674)* mutants have a weak osmotic avoidance phenotype comparable to *nphp-4(tm925)* mutants (Fig. 4 D) but do not exhibit increased lifespan, unlike other cilia gene (e.g., IFT) mutants (Table S1 E). Analysis of *mks-5(tm3100)* mutants uncovered

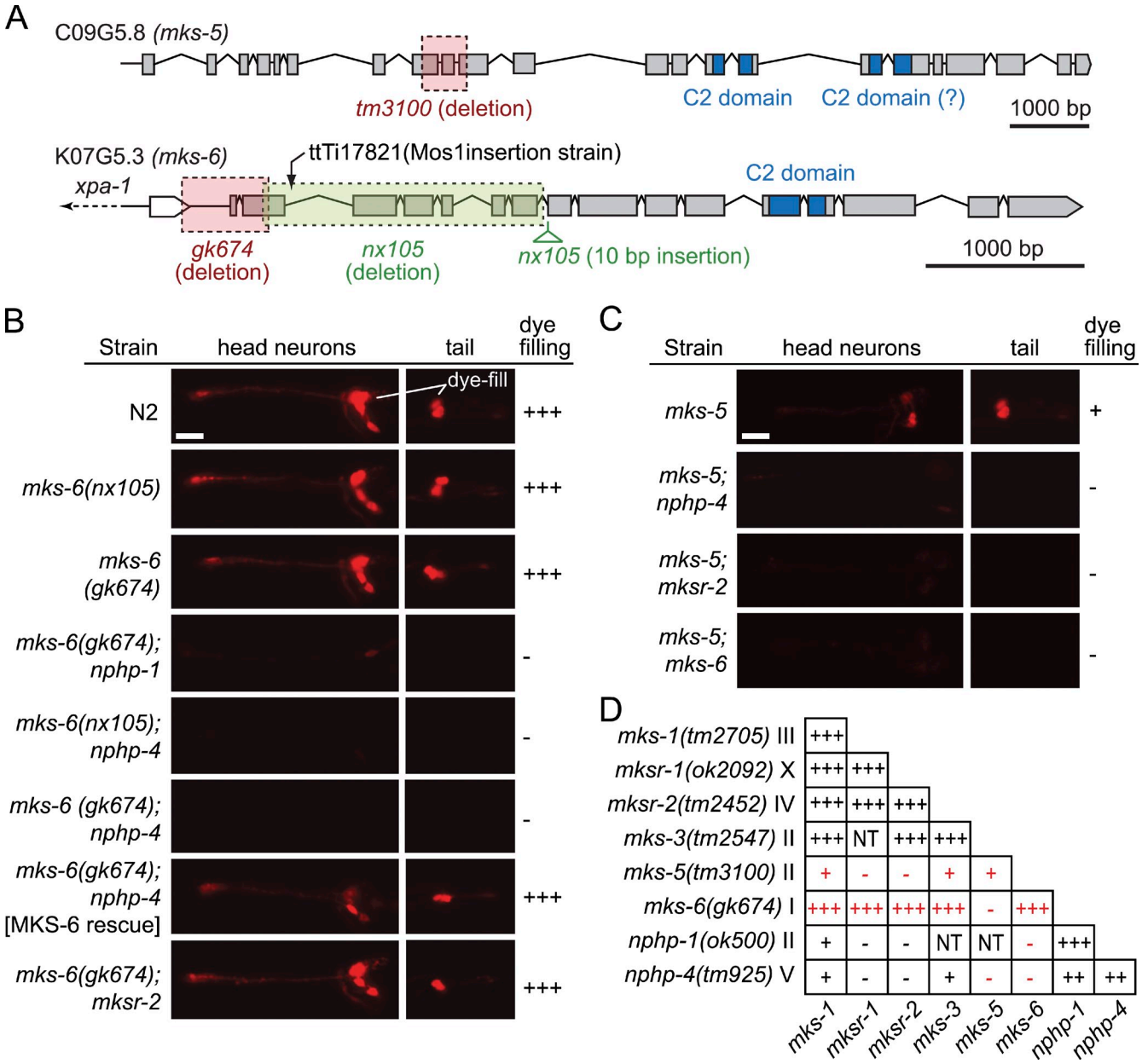

Figure 3. **Functional interactions between MKS-5/MKS-6 and other TZ proteins are required for environmental exposure of cilia to a fluorescent dye, consistent with a role in ciliogenesis.** (A) Gene structures of *C. elegans mks-5* (C09G5.8) and *mks-6* (K07G5.3) and the nature of three deletion alleles, *tm3100*, *gk674*, and *nx105*. (B and C) Representative images of fluorescence staining of environmentally exposed sensory neurons via DiI uptake through cilia in head (amphid) neurons (left panels) and tail (phasmid) neurons (right panels). Dye filling is noted as normal (+++), reduced (+), or absent (−). (B) Wild-type (N2) and *mks-6* strains exhibit normal dye filling; *nphp-1* and *nphp-4* show normal or slightly reduced (++) dye filling (see D; Jauregui et al., 2008). *mks-6;mks-5*, *mks-6;nphp-1*, and *mks-6;nphp-4* double-mutant combinations show little or no dye filling. Expressing GFP-tagged MKS-6 rescues the *mks-6* (double) mutant phenotype. (C) *mks-5(tm3100)* mutants have reduced dye filling, whereas *mks-5;mksr2*, *mks-5;mks-6*, and *mks-5;nphp-4* double mutants show little to no dye filling. Bars, 17.5 µm. (D) Summary of dye-filling phenotypes in single and double *mks/mksr/nphp* mutants. NT, not tested; red, present study; black, data from Jauregui et al. (2008) and Williams et al. (2008, 2010).

moderate defects in dye filling and phasmid (tail) cilia length (Fig. 3, C and D); however, this was not accompanied by prominent changes in either osmotic avoidance, distribution of IFT proteins to BBs/cilia (Fig. 4, A and C; Fig. 5, A, A′, B, and B′), or IFT rates (Table S1 D).

Previously, we found that B9 domain proteins (of the MKS/MKSR module) functionally interact with NPHP-1 and NPHP-4 (NPHP module) to facilitate ciliogenesis (Williams et al., 2008). To determine if similar genetic interactions occur between MKS-5 and MKS-6 and the MKS/MKSR or NPHP modules, we examined *mks-5* and *mks-6* mutations in combination with *mks/mksr* and *nphp* mutations. Compared with wild-type, *mks-5*, *mks-6*, or *nphp-4* single mutants, both *mks-5;nphp-4* and *mks-6;nphp-4* double mutants exhibit strong dye-filling (Dyf) and osmotic avoidance (Osm) phenotypes (Fig. 3, B–D; Fig. 4 D). However, dye filling is normal in *mks-6;mks-1*, *mks-6;mksr-1*, *mks-6;mks-3*, and *mks-6;mksr-2* double mutants (Fig. 3, B and D). These data suggest that *mks-6* genetically

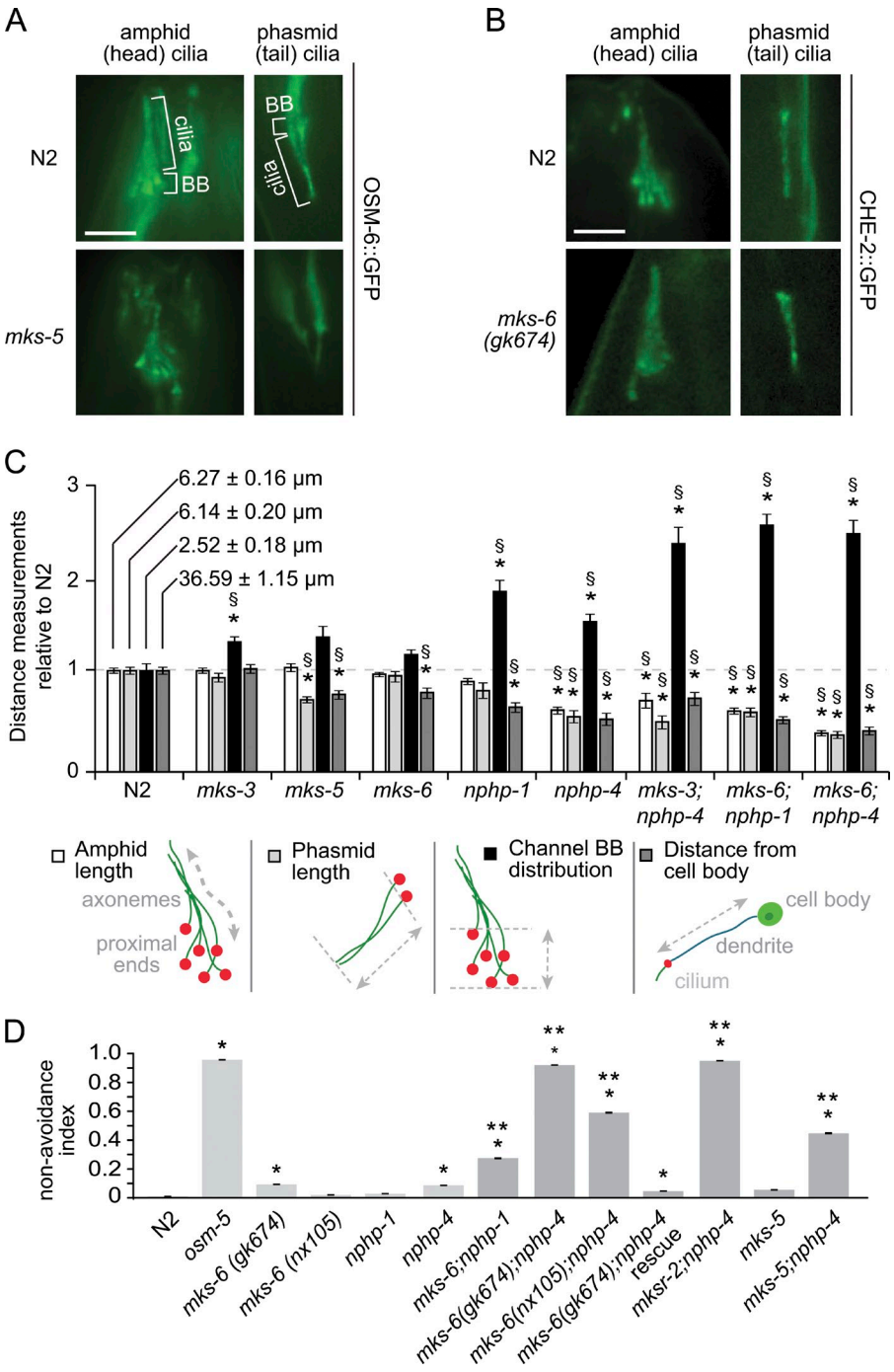

Figure 4. **Functional interactions between TZ proteins are required for correct cilium length and positioning of basal bodies/TZs, as well as chemosensation.** (A and B) Disruption of *mks-5* (A) or *mks-6* (B) has no major effect on the gross morphology/presence of amphid (head) and phasmid (tail) cilia, as revealed by GFP-tagged IFT markers (OSM-6 and CHE-2, respectively). BB, basal body. Bars, 5 µm. (C) Analyses of amphid and phasmid cilia length (white and light gray bars), spatial distribution of BB/TZ in amphid channel neurons (black bars), and position of the BB with respect to the cell body in tail neurons (dark gray bars) are summarized based on phenotypes and statistical analyses shown in Fig. 5. Mean values obtained for wild-type (N2) are shown; *, statistically significant difference ($P < 0.01$) vs. N2; §, statistically significant variance ($P < 0.01$) vs. N2. Schematics illustrate how measurements were made for amphid and phasmid cilia lengths, the distribution of BBs within amphid neurons (some BBs in mutants do not form a tight cluster as in wild type), and distance of the cilia from the phasmid neuron cell body (some mutants have abnormally short dendrites, indicating lack of anchoring of upon retrograde extension of the cell body during development). (D) Graph of cilium-dependent osmotic avoidance of N2 and TZ mutant strains. *osm-5* (control IFT mutant) fails to avoid high osmolarity solution. Two *mks-6* alleles show osmosensation defects in an *nphp-4* mutant background, as do *mksr-2* and *mks-5* mutants. *, significant difference compared with N2 ($P < 0.05$); **, significant difference compared with either single mutant for the indicated double mutant.

interacts with the NPHP module and is associated with the MKS/MKSR module. Interestingly, combining *mks-5* mutants with *mksr-1*, *mksr-2*, or *mks-6* mutations also results in a stronger Dyf phenotype (Fig. 3, C and D), suggesting that *mks-5* genetically associates with not only the NPHP module but also the MKS/MKSR module.

To study in greater detail the ciliary defects of single and double *mks/mksr/nphp* mutants, we used GFP-tagged ciliary (IFT) markers. We uncovered in double mutants multiple phenotypes, including missing or shorter cilia (Fig. 4 C; Fig. 5, A, A′, B, and B′), misoriented cilia (not depicted), and improperly positioned BB/TF regions within the amphid channel and with respect to the phasmid cell body (Fig. 4 C; Fig. 5, C, C′, D, and D′; Williams et al., 2008). Although there is a low penetrance of these phenotypes in *nphp-4* single mutants, they were consistently observed in *mks-6;nphp-4*, *mks-5;nphp-4*, and *mks-6;nphp-1* double mutants (Fig. 4 C; Fig. 5).

Joint disruption of an MKS/MKSR protein and NPHP-4 results in BB/TZ membrane association defects

To assess the nature of the ciliary ultrastructural defects in *mks/mksr/nphp* double mutants, we used TEM. Strikingly, we observed profound and largely indistinguishable phenotypes across

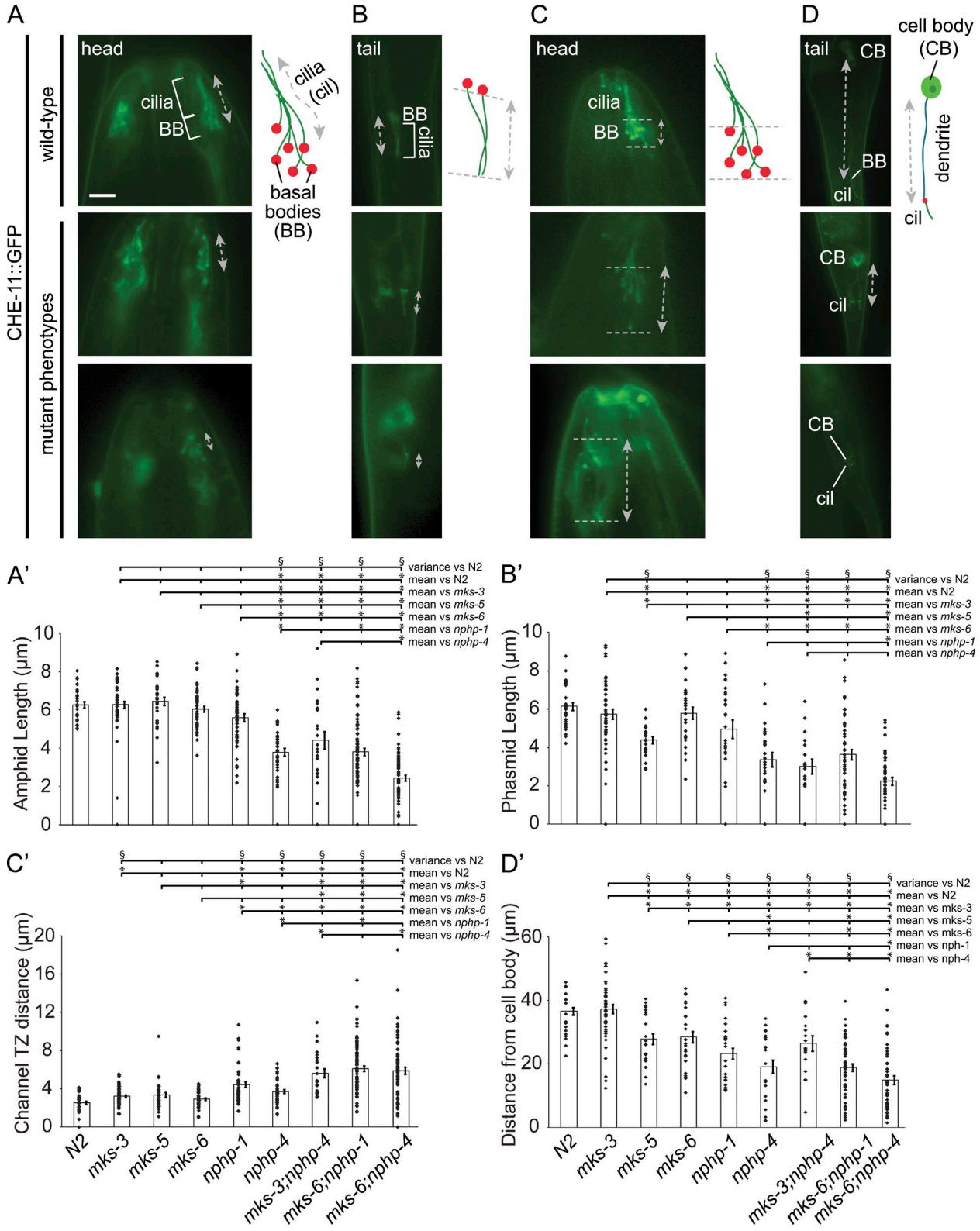

Figure 5. **Detailed analysis of cilia length and positioning in strains with disrupted TZ proteins.** (A–D) Example of correct (wild type; top panels) or defective (for TZ gene mutants; bottom two panels) amphid (A) and phasmid (B) cilia length, distribution of BBs in amphid ciliated neurons (C), and positioning of the BB with respect phasmid neuron cell body (D), using a CHE-11::GFP IFT marker (with the exception of the *mks-5* data, which was obtained using OSM-6::GFP). CB, cell body; cil, cilia; BB, basal body. Bar, 5 µm. (A'–D') Individual data points ($n > 40$) of the measurements in A–D are shown with a bar graph showing average and standard error. Statistically significant differences ($P < 0.01$) in the mean (*) or variance (§) are indicated for all combinations.

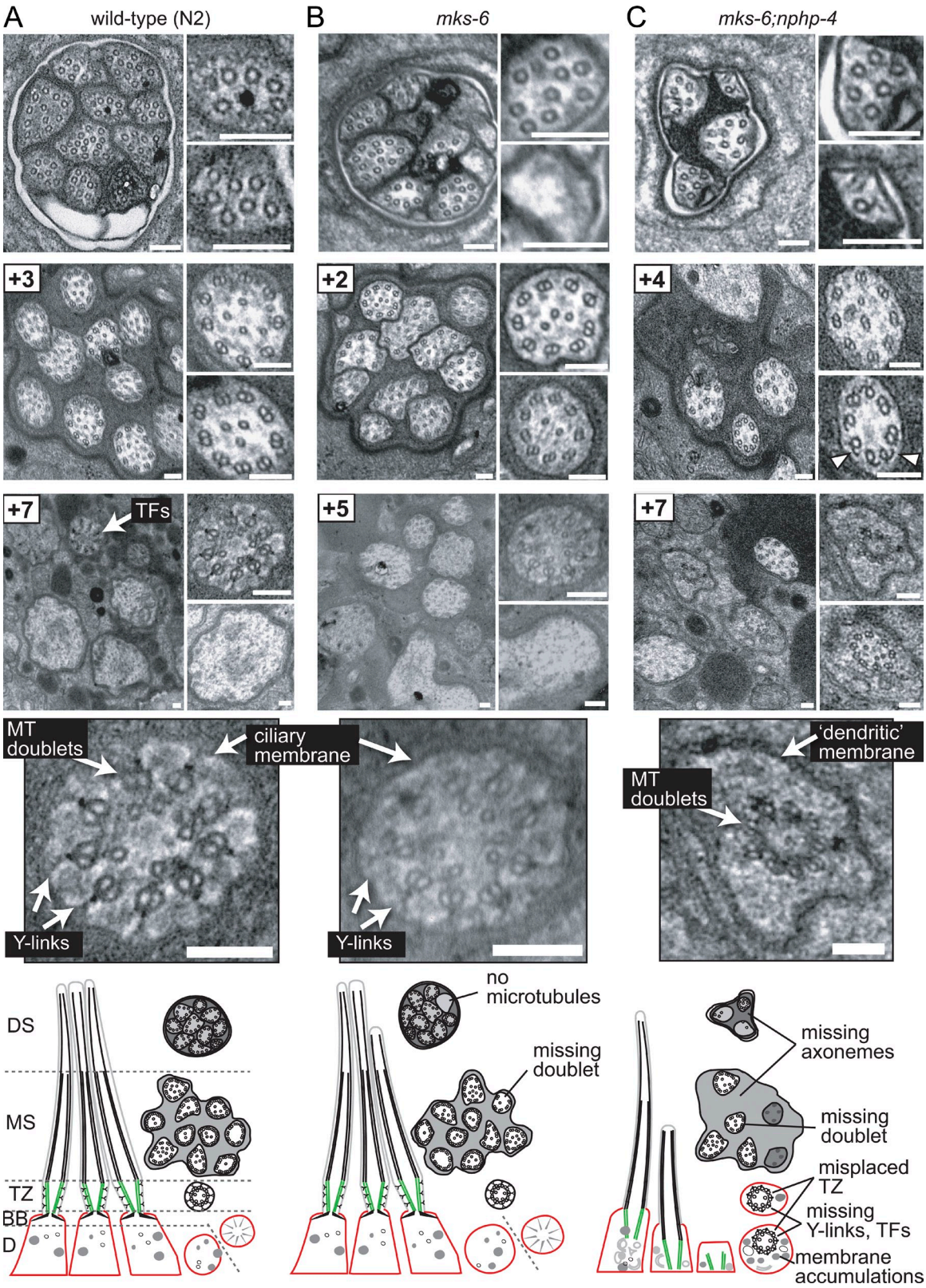

Figure 6. **MKS-6 and NPHP-4 are collectively required for BB/TZ attachments to membrane.** Shown are low and high magnification images from TEM serial cross sections of amphid channel cilia from wild-type (N2), *mks-6*, and *mks-6;nphp-4* worms. Top row, distal segments (DS); middle row, middle segments (MS); bottom row, transition zone (TZ) and distal dendrites (DD). Below bottom row are magnified images of representative TZs. Boxed number denotes proximal positioning of section relative to top section. Schematics (longitudinal, transverse views) summarize the major ultrastructural observations. BB, basal body; TFs, transition fibers. Bars, 100 nm. (A) N2 worms showing 10 singlet microtubule (MT)-containing axonemes in DS, 10 doublets in MS (+3 µm), and TZs (constriction of MT doublets surrounding apical ring) with intact Y-links (connecting doublets with ciliary membrane) anchored at distal dendrite tips (+7 µm). TFs are also observed below this region. (B) Apart from rare axonemes lacking MTs in DS, *mks-6* mutant cilia possess normal DS,

Table I. **Quantification of various ciliary ultrastructure defects in TZ protein–disrupted strains**

Region	Feature/defect	N2	*mks-6*	*mks-6; nphp-4*	*mksr-1; nphp-4*	*mks-1; nphp-4*	*mks-5; nphp-4*	*mks-3; nphp-4*
DS[a]	Ave. axoneme no./pore (*n* = 2–4)	10	10	3	2	6	5	5
	Ave. MT singlet no./axoneme (*n* = 3–44)	8	7	5	7	8	4	6
	No. of axonemes with no MTs[d]	0	4	9	3	8	3	2
MS[b]	Ave. axoneme no./pore (*n* = 2–4)	12	12	5	4	11	9	7
	Ave. MT doublet no./axoneme (*n* = 12–100)	9	8.9	7.7	6.0	8.3	8.0	7.5
	Axonemes with abnormal accumulations[d,e]	0	0	10	0	0	2	0
TZ[c]	Ave. diameter of surrounding membrane (nm) (n′ = 2–34)	260	262	564	436	286	337	320
	Percentage with enlarged membrane diameters (n′ = 2–34)	0	0	100	100	25	100	60
	Percentage of TZs with Y-links (n′ = 2–14)	100	100	0	0	50	0	30
DD	Abnormal vesicle or membrane accumulations[d,e]	0	0	23	4	2	5	4

DS, distal segment; MS, middle segment; TZ, transition zone; DD, distal dendrite; N, number of amphid pores analyzed; *n*, number of axonemes measured; *n*′, number of TZs analyzed.

[a]Singlet microtubule (MT) axoneme region.

[b]Doublet MT axoneme region.

[c]Drawing together of doublet and singlet MTs by the apical membrane; doublets linked to ciliary membrane via Y-links.

[d]As analyses were performed on serial sections, the same axoneme may have been counted multiple times.

[e]Electron-dense accumulations, often vesicular (30–60 nm; often tubular; clear or dense core), sometimes non vesicular (<20 nm).

all double mutants analyzed. Unlike wild-type animals and *mks-6* or *nphp-4* single mutants, which show normal TZs (Fig. 6, A and B; Fig. 7; Jauregui et al., 2008), *mks-6;nphp-4* and *mks-5;nphp-4* double mutants exhibit mispositioned and disrupted TZ regions, with clear disconnections between the BB/TZ region and membrane, accompanied by missing Y-links (Fig. 6 C; Fig. 7; Fig. S1, Fig. S2); hence, their BB/TZ regions are not properly anchored at the distal end of the dendritic membrane. We also observed missing, misplaced, or shorter axonemes, and variably missing TFs. In perhaps the most severe instance of morphological abnormality, *mks-5;nphp-4* double mutants had incomplete TZ microtubule rings (Fig. S2). Phenotypes nearly identical to *mks-6;nphp-4* mutants were observed in the *mksr-1;nphp-4* strain (Fig. 7; Fig. S3). The various cilia defects uncovered by TEM are quantified in Table I. Notably, all TZ/cilia anomalies are in addition to open tubules observed in the *nphp-4* mutant (Jauregui et al., 2008) and are distinct from those of IFT and other cilia mutants, in which TZ regions are intact (Perkins et al., 1986).

Given the severe ciliary phenotypes of *mks-5;nphp-4* and *mks-6;nphp-4* strains, we wondered if *mks-1;nphp-4* and *mks-3; nphp-4* mutants, which have milder Dyf phenotypes (Williams et al., 2008, 2010), would present with similar—yet partial or more specific—ultrastructure defects. Although similar ciliary defects were observed in the latter mutants (Fig. 7; Fig. S4, Fig. S5), some of their TZ regions are in normal proximity to the ciliary membrane but often lack connecting Y-links; this raises the possibility that MKS/MKSR/NPHP proteins comprise components of these structures or are required for their stability.

TZ proteins participate in early ciliogenesis independent of IFT-associated proteins

Our data indicate that MKS/MKSR/NPHP proteins are important for BB/TZ interactions with the membrane, which likely occur during ciliogenesis before IFT-dependent axoneme extension, suggesting a role in an early step of the ciliogenic pathway (Sorokin, 1968). To test if this early step depends on IFT, we looked for IFT defects using kymograph analyses in *mks/mksr/nphp* double mutants where a small proportion of cilia still form. Remarkably, IFT was largely unaffected in these double (as well as single) mutants (Table S1 D; Bialas et al., 2009), in striking contrast to *C. elegans* IFT mutants where disruption of anterograde or retrograde IFT occurs (Hao and Scholey, 2009), or BBS mutants (*bbs-1/7/8*), where stability/association of IFT subcomplexes A and B is compromised (Blacque et al., 2004; Ou et al., 2007). Because no TZ phenotypes observed in our study are apparent in IFT or BBS mutants (Perkins et al., 1986; unpublished data), and because IFT is largely unaffected, we propose that NPHP and MKS protein modules act before IFT-driven axoneme formation. From this model we predict that the TZ should be established properly when IFT is disrupted. This was validated in IFT and BBS mutants, where MKS-6 (Fig. 8 F) and other MKS/NPHP proteins (unpublished data) localize normally to the TZs of cilia lacking fully formed axonemes. Together, these data support a model where TZ proteins function in an early ciliogenic step (BB/TZ association with membrane) followed by a subsequent IFT/BBS-dependent step in axoneme elongation/trafficking.

MS (+2 µm), and TZ (+5 µm) regions. (C) In DS and MS (+4 µm) regions of *mks-6;nphp-4* worms, many axonemes are missing and amphid pore size is reduced. Open/unzipped B-tubules are also observed, as in *nphp-4* mutants (Jauregui et al., 2008). In TZ/DD region, TZs are not anchored at the membrane of the DD tips, but instead are often mispositioned in more proximal regions of the dendrites (see also schematic). Y-links at the TZ are missing and TFs are not observed.

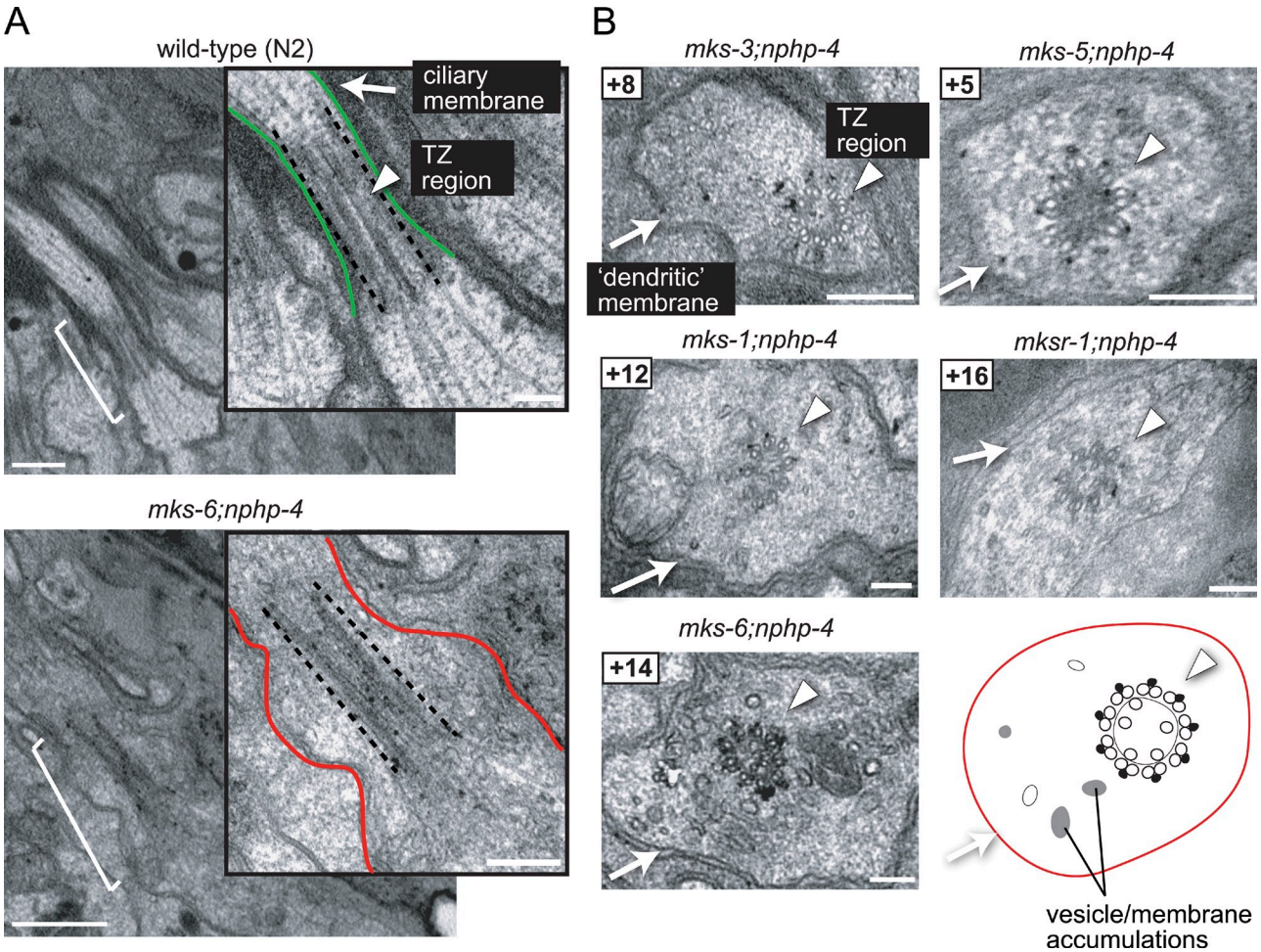

Figure 7. **Functional interactions between five TZ-associated proteins (MKS-1, MKSR-1, MKS-3, MKS-5, and MKS-6) and NPHP-4 contribute to anchoring the BB/TZ to membrane.** (A) TEM images of amphid channel TZ regions obtained from longitudinal sections of wild-type (N2) and *mks-6;nphp-4* double mutants. Compared with N2 worms in which membrane (green outlines) associates tightly with the TZ (demarcated by dashed lines), *mks-6;nphp-4* double-mutant TZs fail to anchor to the surrounding membrane (red outlines). Bars, 500 nm; 200 nm (insets). (B) TEM images of amphid channel ciliary TZ regions obtained from cross sections of *mks-3;nphp-4*, *mks-5;nphp-4*, *mks-1;nphp-4*, *mksr-1;nphp-4* and *mks-6;nphp-4* double mutants. Boxed number denotes the proximal positioning of the imaged section relative to the most distal sections of the amphid pore. In all worms, the MT doublet-containing TZ ring is not anchored at distal dendrite tips (which are typically positioned at +5 to +6 µm relative to distal amphid pore); instead, TZs are found at abnormal proximal positions in the dendrites (+8 to +16 µm). Y-links are frequently not observed. Bars, 100 nm.

MKS-5 is a central component required for docking/anchoring MKS and NPHP protein modules

Our TEM analyses provide fundamental insights into defects caused when TZ proteins (MKS-1, MKSR-1, MKS-3, MKS-5, and MKS-6) are disrupted jointly with NPHP-4 (Figs. 6 and 7; and Figs. S1–S5). The ultrastructural defects overlap greatly between mutants, implying a shared function for MKS/MKSR/NPHP proteins. Further support comes from biochemical data linking many ciliopathy proteins in shared macromolecular complexes (Table S1 A). To provide further evidence for shared/modular functions, we queried whether disrupting particular TZ proteins affected the localization of others. Using this approach, we rule out MKS-1, MKS-3, MKS-6, and NPHP-1 as critical docking proteins, as their disruption had no effect on localization of other TZ proteins (Fig. 8, B–F; Winkelbauer et al., 2005; Williams et al., 2008, 2010). In contrast, disrupting MKSR-1, MKSR-2, or MKS-5 results in TZ delocalization of MKS-6 (Fig. 8 B) and MKS-3 (Fig. 8 C, Fig. 9 L). Furthermore, *mks-5* mutants failed to properly localize MKS-1, MKSR-1, and MKSR-2, suggesting a key role of MKS-5 in docking proteins at the TZ (Fig. 8 C). Notably, NPHP-1 and NPHP-4 localization was also altered in *mks-5* mutants (Fig. 8 C), albeit differently; instead of failing to anchor at the TZ, NPHP-1 and NPHP-4 occupied a smaller region than wild-type animals (TZ length of 0.65 µm, $n = 19$ in *mks-5* mutants vs. 1.05 µm, $n = 23$ in controls; t test $P < 0.0001$). MKS-5 was unaffected upon disruption of MKSR-2 or NPHP-4, which are otherwise required for TZ docking most other MKS/MKSR proteins and NPHP-1, respectively (Fig. 8 D; Winkelbauer et al., 2005; Williams et al., 2008). Moreover, MKS-5 is still TZ localized in *mks-6;nphp-4* double mutants in which ciliary microtubule–membrane attachments are disrupted (compare Fig. 8 D with Fig. 8 E, in which transmembrane MKS-3 is predictably lost in the same double mutant). Thus, we conclude that MKS-5 localizes to the TZ independently of other TZ proteins tested and performs a central role as a scaffold for anchoring other MKS/MKSR and NPHP module proteins.

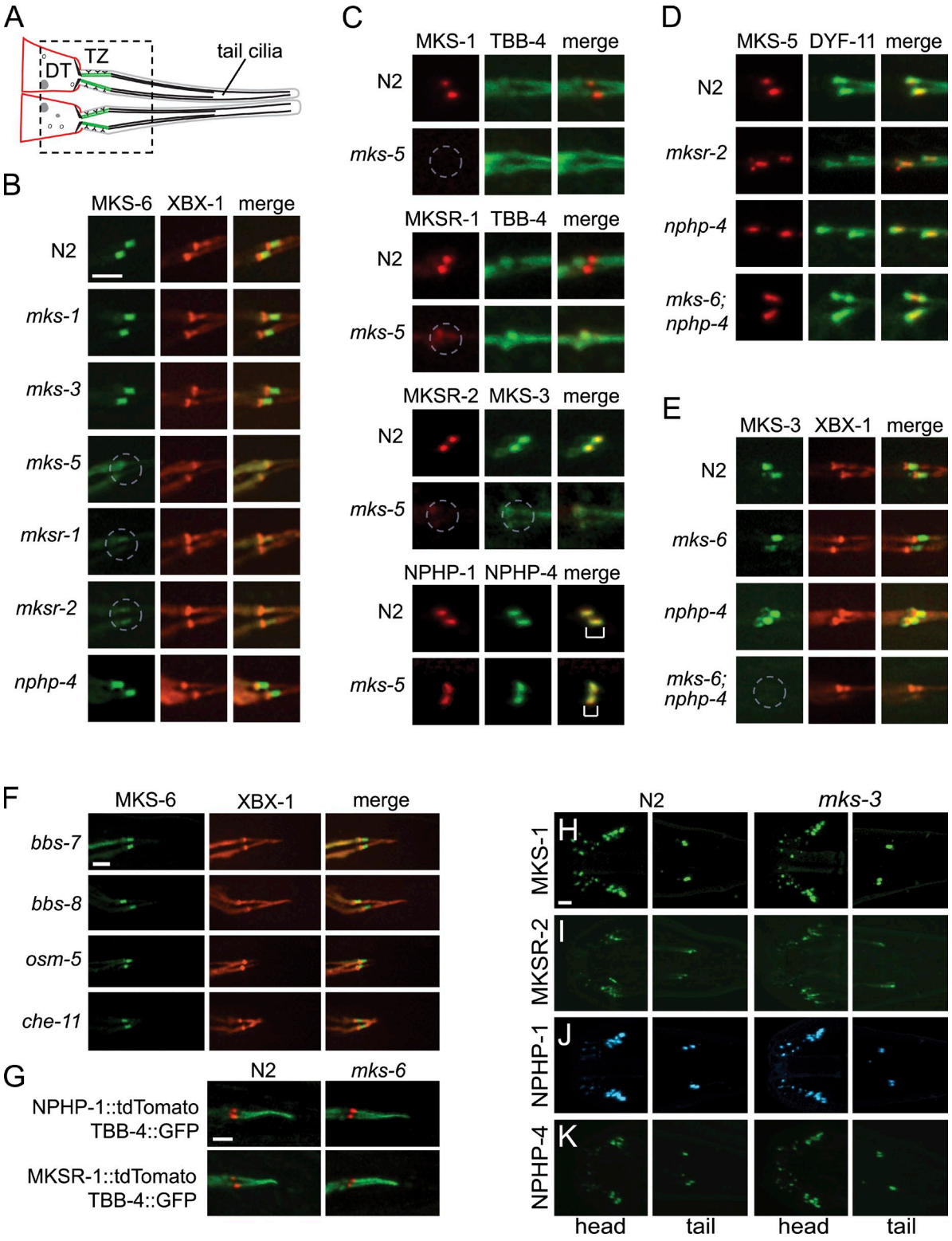

Figure 8. **MKS/MKSR and NPHP proteins are organized hierarchically as modules, and independently of IFT/BBS proteins, at the TZ.** (A) Schematic representing the region of phasmid (tail) cilia analyzed in B–E. Entire cilia/cilia regions are shown in F–K. (B–E) Co-dependent localization of fluorophore-tagged TZ proteins. TZs lacking normal localization of a particular protein are circled. (B) MKS-6::GFP localizes normally in wild-type (N2) and *mks-1*, *mks-3*, and *nphp-4* mutants, but mislocalizes in *mks-5*, *mksr-1*, and *mksr-2* mutants. (C) *mks-5* mutants fail to localize MKS-1, MKSR-1, MKSR-2, and MKS-3, the latter dispersing along the cilium axoneme (see also Fig. 9 L). NPHP-1 and NPHP-4 localize to the TZ in *mks-5* mutants, but to a subregion smaller than that occupied in N2 (compare brackets). (D) MKS-5::tdtomato localization at the TZ is not perturbed in *mksr-2, nphp-4,* or *mks-6;nphp-4* double mutants. (E) MKS-3::GFP localizes correctly to the TZ in *nphp-4* and *mks-6* single mutants but is mislocalized in the double mutant. (F) MKS-6::GFP localizes normally in *bbs* mutants (*bbs-7, bbs-8*) and *ift* mutants (*osm-5, che-11*), indicating the presence of an intact TZ. (G) tdTomato-tagged NPHP-1 (top) and MKSR-1 (bottom) localize normally at the TZ in *mks-6(gk674)* mutants. (H–K) CFP- or YFP-tagged MKS-1, MKSR-2, NPHP-1, and NPHP-4 localize normally at the TZ in *mks-3* mutants. Bars, 2.5 µm.

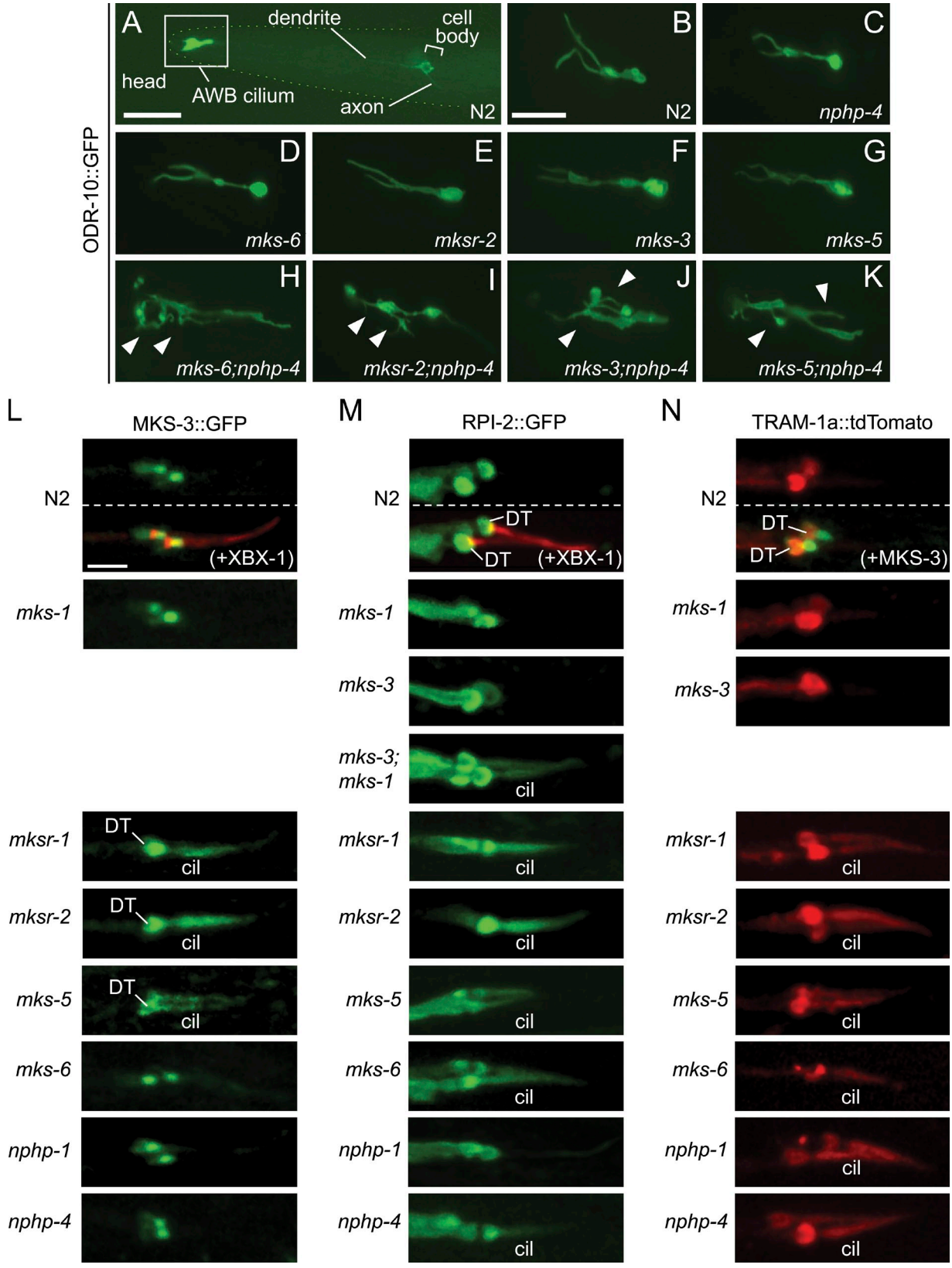

Figure 9. **MKS/NPHP proteins are required for ciliary gate function but not for ODR-10 trafficking.** (A and B) GFP-tagged ODR-10 odorant receptor concentrates specifically at the AWB cilium in wild-type (N2) animals, showing a typical branched ciliary structure. Bars: (A) 25 µm; (B–K) 8 µm. (C–G) Disruption of the indicated TZ genes does not overtly affect the structure of the AWB cilium or presence of ODR-10::GFP. (H–K) Various double TZ mutants reveal abnormal AWB ciliary structures but otherwise normal localization of ODR-10::GFP to the ciliary membrane. (L) MKS-3::GFP localizes normally at the TZ in *nphp-1* and *mks-1* mutants but accumulates abnormally inside cilia (cil) and at dendritic tips (DT) in *mks-5, mksr-1,* and *mksr-2* mutants. Bar, 2.5 µm. (M) GFP-tagged RPI-2 is found at dendritic tips but not inside cilia, marked by XBX-1::tdTomato in wild-type worms. RPI-2 localizes normally in *mks-1, mks-3,*

TZ proteins are not required for trafficking of a cilium-targeted protein

Given the presence of C2 domains in MKS-5 and MKS-6 and related B9 domains in MKS-1, MKSR-1, and MKSR-2, we hypothesized that these proteins may be required for vesicle trafficking and/or docking/fusion of vesicles harboring ciliary cargo at the TZ (Nalefski and Falke, 1996). Thus, we used a well-established odorant receptor (ODR-10; Sengupta et al., 1996) as a functional marker for vesicular trafficking to cilia. In wild-type animals, ODR-10 (expressed under the *str-1* promoter) concentrates at the branched AWB cilium membrane (Fig. 9, A and B). In single TZ mutants, no apparent defects in cilia structure or ODR-10 localization are seen (Fig. 9, C–G). Although AWB cilium morphology in TZ double mutants is compromised, ODR-10 localization to its ciliary membrane appears normal (Fig. 9, H–K). These findings suggest that TZ proteins do not play an essential role in ciliary cargo-associated vesicle trafficking to, and docking/fusion steps at the base of cilia.

TZ proteins establish a gate that modulates ciliary composition

Our analyses uncovered important roles for MKSR-1, MKSR-2, and MKS-5 in TZ localization of the transmembrane protein MKS-3 (Fig. 8 C; Fig. 9 L). Interestingly, in addition to being lost from the TZ in *mksr-1*, *mksr-2*, and *mks-5* mutants, MKS-3 accumulates along ciliary axonemes (and at nearby dendritic tips; Fig. 9 L). This indicates that MKSR-1, MKSR-2, and MKS-5 restrict MKS-3 to the TZ membrane. Based on these observations, we wondered if other membrane-associated proteins (in particular, non-TZ-associated proteins) also accumulate in cilia when TZ proteins are disrupted. We examined RPI-2, the *C. elegans* orthologue of human X-linked retinitis pigmentosa 2 (RP2; Schwahn et al., 1998; Chapple et al., 2000). In wild-type *C. elegans*, GFP-tagged RPI-2 associates with membrane in sensory neurons, enriched as a ring-like pattern near or at BB/TFs (Blacque et al., 2005), as in trypanosomes (Stephan et al., 2007), but not within cilia (Fig. 9 M). In contrast, we observed that in TZ mutants, RPI-2 accumulates inside cilia (Fig. 9 M). We acquired almost identical results with the transmembrane protein TRAM-1a (Fig. 9 N), which in wild-type animals is found at dendritic tips and excluded from cilia (Bae et al., 2006). Together, our data showing abnormal accumulations of MKS-3, RPI-2, and TRAM-1a in TZ mutant cilia indicate that, in addition to their role in early ciliogenesis, most if not all TZ proteins normally function to maintain a boundary at the cilium base, establishing the TZ as a bona fide ciliary gate.

Discussion

Modular function reduces the perceived complexity of heterogeneous disorders

There are at least 35 genes associated with primary cilia disorders (Baker and Beales, 2009). Several, including *BBS* genes, are linked to IFT (Blacque and Leroux, 2006; Beales et al., 2007), but most lack clearly assigned molecular functions. Many of these components display genetic and/or physical interactions and are associated with overlapping clinical ailments, suggesting involvement in a common cellular process.

Our findings indicate that *C. elegans* proteins implicated in many ciliopathies, including MKS, NPHP, JBTS, and LCA, function at the TZ and are required for BB and TZ attachment to the membrane and establishing a ciliary gate early in ciliogenesis (Fig. 10 D). Assignment of individual proteins to a particular TZ module (MKS/MKSR or NPHP) simplifies our understanding of the associated ciliopathies. Although previously seen as diseases of complex and seemingly unrelated molecular etiology, our data indicate that MKS and NPHP are likely disorders of macromolecular complexes sharing a common biological function. This is similar to the finding that several BBS proteins are constituents of the multimeric BBSome, which functions as a ciliary coat complex (Nachury et al., 2007; Jin et al., 2010). Indeed, a collective function of TZ proteins is supported by fragmented but increasing biochemical data in mammalian systems (Fig. 10 A; Table S1 A). Other functional modules/complexes may have disparate yet essential ciliary functions that are associated with equivalent ciliopathies; one likely includes NPHP2/inversin, NPHP3, and NEK8, which localize at the Inv ciliary compartment just distal to the TZ (Shiba et al., 2010).

A hierarchical, modular interaction network involving TZ proteins

We propose that MKS/MKSR and NPHP proteins form a hierarchical network comprised of distinct modules with partial functional redundancy (Fig. 10, B and C). The rationale for this modular hypothesis stems from our findings that in *C. elegans*, synthetic ciliary defects result from mutations in at least two TZ genes—but not any two genes (Fig. 3, B–D; Figs. 4–7). For example, even triple B9 gene (*mks-1*, *mksr-1*, and *mksr-2*) or *nphp-1;nphp-4* double mutants lack prominent (additive) ciliary defects (Jauregui et al., 2008; Bialas et al., 2009). In contrast, disrupting any B9 gene together with *nphp-1* or *nphp-4* results in severe cilia anomalies (Williams et al., 2008). Other mutant combinations such as *mks-1;mks-3*, or *mks-6*;*mksr-2,* do not noticeably disrupt cilia, whereas the same four individual mutants show strong genetic interactions with *nphp-1* or *nphp-4* (Fig. 3, B–D; Figs. 4–7). Thus, we group MKS-1, MKSR-1, MKSR-2, MKS-3, and MKS-6 into an MKS/MKSR module and NPHP-1 and NPHP-4 into an NPHP module (Fig. 10 C). Importantly, MKS-5 represents an exception to this module assignment. Disrupting *mks-5* together with *mksr-1*, *mksr-2*, *mks-6* (MKS/MKSR module), or *nphp-4* (NPHP module) compromises cilia morphology (Fig. 3, B–D). Moreover, *mks-5* mutants fail to localize MKS-1, MKSR-1, MKSR-2, MKS-3, and MKS-6 (i.e., the entire known MKS/MKSR module) to the TZ;

and *nphp-1* single mutants but accumulates within cilia of *mks-3;mks-1* double mutants and *mksr-1, mksr-2, mks-5, mks-6,* and *nphp-4* single mutants. Bar, 2.5 µm. (N) tdTomato-tagged TRAM-1a is found at dendritic tips but not inside cilia (ciliary TZ marked by MKS-3::GFP) in wild-type worms. TRAM-1a localizes normally in *mks-1* and *mks-3* mutants but accumulates within cilia of *mksr-1, mksr-2, mks-5, mks-6, nphp-1,* and *nphp-4* mutants. Bar, 2.5 µm.

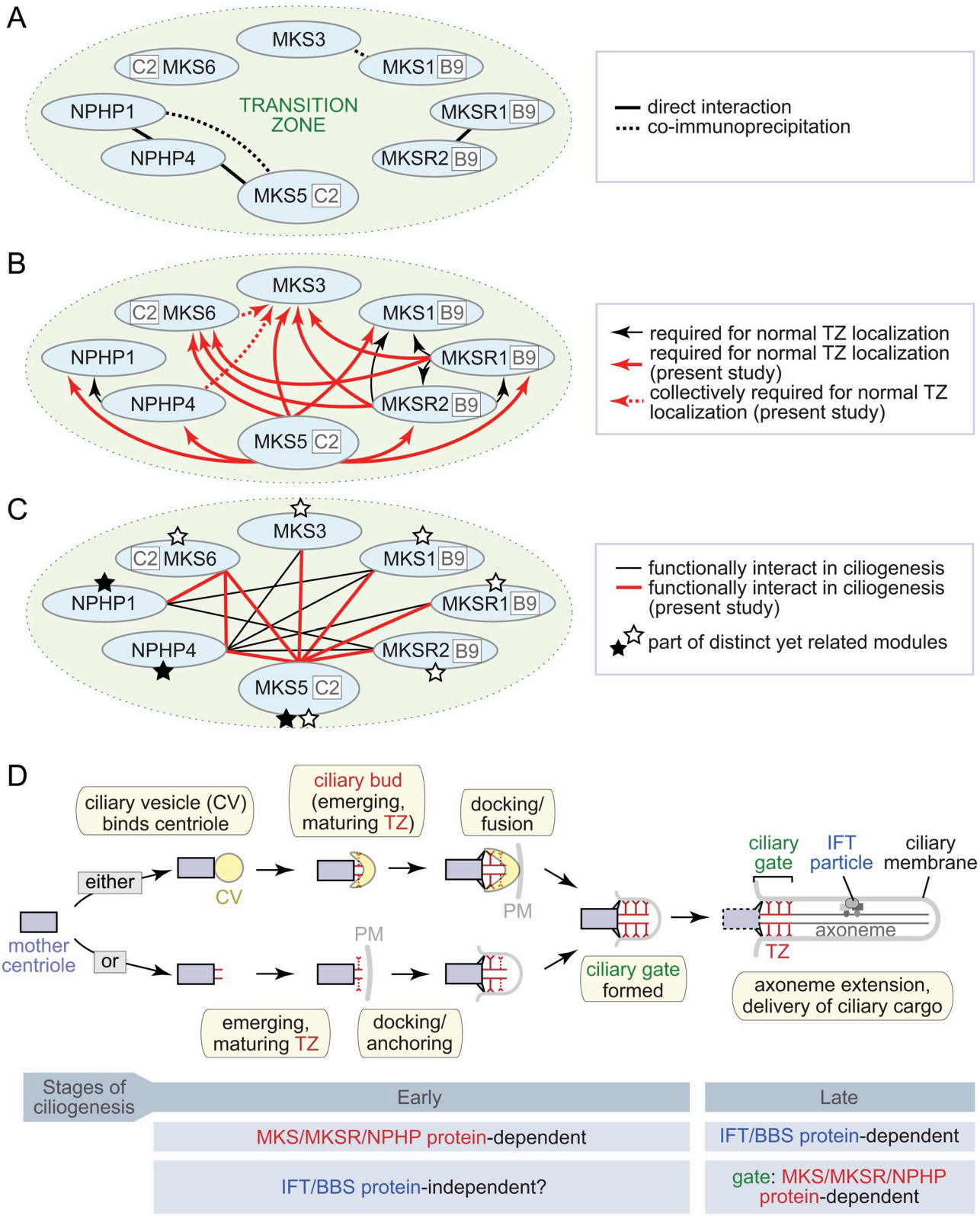

Figure 10. **MKS/MKSR and NPHP proteins form part of a functional interaction network required for an early stage of ciliogenesis and formation of an intact ciliary gate.** (A) Previously identified physical interactions between *C. elegans* or mammalian TZ proteins (see also Table S1 A). Interactions between MKS1 and MKS3 and between NPHP1, NPHP4, and MKS5 were identified in mammals. The interaction between MKSR1 and MKSR2 was identified in *C. elegans*. (B) Summary of hierarchy analysis uncovering the requirement of some TZ proteins for normal localization of others. Black arrows represent previously known requirements (arrows point away from the protein required for localization of the other). Red arrows represent novel requirements uncovered in this study. (C) Summary of functional (genetic) interactions between *C. elegans* TZ components influencing ciliogenesis. Black lines represent previously known functional interactions, and red lines represent genetic interactions uncovered in this study (dye-filling/ciliogenesis and/or BB docking/anchoring and ciliary structures, as revealed by TEM). Modular assignments based on these functional interactions and hierarchy analysis data are represented by

the *mks-5* mutation also partially alters NPHP-1 and NPHP-4 distribution at the TZ (summarized in Fig. 10 B). Based on our data, we propose that the MKS/MKSR and NPHP modules are functionally linked through MKS-5 (Fig. 10 C). Whether the modules are physically associated together at the TZ remains to be examined; however, the established biochemical interaction between mammalian MKS5/RPGRIP1L and NPHP4 (Roepman et al., 2005) indicates this is likely. Further, the likelihood that MKS-5 links multiple functional modules is supported by the finding that human *RPGRIP1L* mutations contribute to at least six distinct ciliopathies, including MKS and NPHP (Zaghloul and Katsanis, 2010).

The genetic interactions we observe in *C. elegans* also likely exist between TZ genes in mammals. For example, *RPGRIP1L* and *CEP290* heterozygous variants are linked to increased phenotypic pleiotropy in some NPHP patients in which primary disease symptoms are caused by mutations in other genes (Tory et al., 2007; Khanna et al., 2009). Our findings may also help explain data reported by Hoefele et al. (2005), who screened human NPHP patients and determined that single heterozygous mutations in *NPHP4* were over three times more prevalent than two recessive mutations. Based on our genetic interaction studies in *C. elegans*, we predict that the ailments in these patients result from interactions between mutations in other TZ module genes. With the growing number of available MKS and NPHP rodent models, such possibilities could be formally examined by assessing the consequences of combining mutant alleles of multiple TZ genes.

Intriguingly, proteins seemingly absent in *C. elegans* or *Drosophila* have recently been implicated in BB- or TZ-associated functions in other organisms. These include the Ahi1 ciliopathy protein, which binds RAB8 and is proposed to play a role in polarized membrane trafficking (Hsiao et al., 2009), as well as OFD1 and Talpid3, which may assist with docking the ciliary vesicle onto the centriole (Yin et al., 2009; Singla et al., 2010). Another such protein is CEP290, which binds MKS6 (Gorden et al., 2008) and thus likely functions in the MKS or NPHP module. CEP290 was assigned as a component of Y-links and ciliary gate in *Chlamydomonas* (Craige et al., 2010), and mutations in this gene occur in several ciliopathies. Whether CEP290 functionally interacts with other TZ proteins to facilitate BB/TZ membrane attachments in an early ciliogenic event—as we have shown in this study for several evolutionarily conserved TZ proteins—remains to be determined.

TZ vs. BB

The TZ is an underappreciated ciliary subcompartment, often incorrectly presumed to be one and the same with the adjacent BB. This misconception was inadvertently strengthened by Keller et al. (2005), who identified constituents of the *Chlamydomonas* "basal body" proteome; however, in these analyses the TZ was co-isolated with the BB. Thus, some TZ proteins (e.g., CEP290, NPHP4) were ascribed to the BB, leading to the widespread belief that NPHP and MKS are diseases of BB dysfunction.

Confusion regarding differences between the *C. elegans* BB and TZ is also apparent. As *C. elegans* lacks classical BB microtubule architecture at the base of cilia (Perkins et al., 1986), similar to that observed in mature murine sperm (Manandhar et al., 1998), it has long been speculated that the nematode TZ is "analogous" to the BB. However, several observations suggest this is inaccurate. First, in *daf-19* mutants, which lack TZs and cilia, typical centriolar pairs are observed unattached to distal dendritic membranes where cilia would normally form (Perkins et al., 1986). Second, TFs present at the base of *C. elegans* cilia (Fig. 1 A; Perkins et al., 1986) are evolutionarily conserved structures present at the distal end of all BBs (Silverman and Leroux, 2009). Third, the conserved centriolar/BB protein HYLS-1 localizes in *C. elegans* within the TF region, just proximal to NPHP-4 at the TZ (Dammermann et al., 2009). Importantly, HYLS-1 in *C. elegans* and vertebrates is dispensable for centriole function during cell division but critical for ciliogenesis (Dammermann et al., 2009). We propose that the *C. elegans* TF region, where different IFT proteins concentrate—as shown for IFT52 in *Chlamydomonas* (Deane et al., 2001)—functions as a bona fide BB that is adjacent to but distinct from the TZ, where MKS/MKSR/NPHP proteins localize (Fig. 1 A, B–D; Fig. 2). Further, our finding that Y-links are completely, or even selectively, lost in MKS/MKSR/NPHP double mutants leaves open the possibility that at least some of these proteins represent structural elements (e.g., Y-links) of the TZ. Indeed, structural and biochemical properties of various MKS/MKSR/NPHP proteins support this possibility; NPHP1 binds microtubules (Otto et al., 2003), the C2/B9 domain proteins are predicted to associate with the inner leaflet of the plasma membrane, and MKS3 is membrane spanning. Taken together, one begins to envision two or more MKS/MKSR/NPHP modules—likely joined by MKS5—as components of the Y-link/ciliary necklace structures that connect axonemal microtubules to the surrounding membrane.

TZ-dependent establishment of the ciliary gate

Our analyses revealed that MKS/MKSR and NPHP modules are collectively required for two essential aspects of ciliogenesis, namely membrane anchoring of the BB/TZ and formation of an intact TZ region. Through these processes, the ciliary gate is

stars. (D) Model depicting early and late events in ciliogenesis, first involving transition zone (TZ) proteins and then IFT-associated proteins. Top pathway: in some mammalian cell types, the earliest step of ciliogenesis involves binding of a ciliary vesicle (CV) to the mother centriole, followed by migration of the centriole-CV toward the plasma membrane (PM). At some point a ciliary bud (likely to be a maturing TZ) emerges, invaginating the CV. Bottom pathway: in other cells, the CV may be expendable, and docking of the centriole/developing TZ occurs directly with the PM. During these early steps, interactions between the BB and TZ with the membrane depend on MKS/MKSR/NPHP TZ proteins. Assembly of the TZ in early ciliogenesis likely coincides with formation (of at least part) of the ciliary gate, and MKS/MKSR/NPHP proteins are functional/structural elements of this mechanism. IFT and BBS proteins are not necessary for formation of the TZ or for BB/TZ anchoring to the membrane during early ciliogenesis, but after these events IFT proteins participate in building (and maintaining) the rest of the ciliary axoneme, and BBS proteins participate in the delivery of ciliary cargo.

established (Fig. 10 D). The observed axoneme extension defects in TZ double mutants probably arise as a secondary consequence of anomalies in these early ciliogenic events.

The TZ in early ciliogenesis. Largely normal IFT rates in TZ mutant strains, and the fact that IFT mutants do not display phenotypes comparable to those of TZ mutants by TEM analysis (Perkins et al., 1986), support the notion that IFT proteins play a role in ciliogenesis distinct from that of TZ proteins, namely building the axoneme and delivering ciliary cargo vs. microtubule-membrane association/stabilization (Fig. 10 D). This difference is reflected in rodent models in which IFT perturbation (cilia ablation) causes early embryonic lethality (at ∼E8.5–10.5), whereas disrupting MKS/MKSR/NPHP proteins leads to less severe ciliogenesis defects and developmental outcomes (Murcia et al., 2000; Jiang et al., 2009; Tammachote et al., 2009). TEM studies of mammalian cells forming cilia (Sorokin, 1962) are consistent with a possible role for the TZ in early ciliogenesis (Fig. 10 D). Specifically, an early ciliogenic step involves the interaction of a Golgi-derived "ciliary" vesicle (CV) with the distal end of the mother centriole/nascent BB to establish microtubule–membrane associations. A "ciliary bud" grows from the centriole, invaginating the CV, which itself appears to grow by fusion with secondary vesicles. In all likelihood, the ciliary bud, visible before BB docking/anchoring with the plasma membrane (Sorokin, 1962; Moser et al., 2010), represents a developing TZ; i.e., the first section of the ciliary axoneme (Fig. 10 D; Rohatgi and Snell, 2010). After docking and fusion with the membrane, the ciliary bud/TZ further extends to form the ciliary axoneme, a step dependent on IFT proteins. Alternatively, in other cell types, the centriole/TZ may dock directly with the plasma membrane, forgoing association with a CV; in this instance, microtubule–membrane associations mediated through the TZ also occur before axoneme extension (Fig. 10 D).

The TZ ciliary gate. The ciliary gate was long thought to be important in cilia function (Rosenbaum and Witman, 2002), but is only now being studied at the molecular level (Jauregui et al., 2008; Craige et al., 2010). The BB/TZ region is thought to facilitate ciliary gate function as a docking site for proteins destined for the cilium, as a region of selective active transport, and as a diffusion barrier. We demonstrate that individual MKS/MKSR and NPHP-disrupted strains lack a normal ciliary barrier, as evidenced by accumulation of nonciliary proteins within cilia. Alternatively, these proteins may enter cilia at low levels normally and instead require NPHP and MKS proteins for efficient removal from the compartment. Regardless, our data indicate that MKS/MKSR/NPHP proteins establish the TZ as a ciliary gate, and we predict that these TZ proteins likely function in coordination with other mechanisms—including IFT, the Ran-importin system, and BBSome (Bae et al., 2006; Jauregui et al., 2008; Craige et al., 2010; Dishinger et al., 2010; Jin et al., 2010)—to control cilium composition and thus function.

Concluding remarks

Ciliopathies are genetically heterogeneous but have overlapping phenotypic presentations, suggesting a common cellular mechanism as the basis of their etiology. In this study, we show that eight *C. elegans* proteins jointly function in establishing connections between the ciliary membrane and axoneme at the TZ, and in formation of the ciliary gate to regulate ciliary membrane composition. These TZ proteins are highly conserved in ciliated organisms (Hodges et al., 2010), suggesting that our model will be widely applicable.

Materials and methods

Strains and general methods

All strains (Table S1 B) used were maintained and cultured at 20°C using standard techniques (Brenner, 1974). Many procedures used in this study are summarized in Inglis et al. (2009). *K07G5.3(gk674)* and *C09G5.8(tm3100)* worms were obtained from the knockout consortium (http://celeganskoconsortium.omrf.org) and the National Bioresource Project (Japan), respectively, and outcrossed 5x to wild type. Because the *gk674* deletion removes some neighboring *xpa-1* gene sequence (Fig. 3 A), we confirmed that the nonciliary function of this DNA repair gene was not abrogated. First, the lifespan of the available *xpa-1(mn157)* mutant is shorter (P<X) than N2 worms, whereas *gk674* mutants are wild type for lifespan (Table S1 E). Second, *xpa-1* animals, but not *gk674* or N2 worms, possess defective DNA repair as observed by UV irradiation dose-killing curves.

To generate a null allele for *K07G5.3*, we used PCR to screen for imprecise excision events from ttTi17821 worms, which contain a Mos1 transposon inserted in K07G5.3 (Fig. 3 A). The mutagenesis protocol, modified from Boulin and Bessereau (2007), is as follows. Strain EG1642 (*lin-15B(n765)X*; oxEx166[HSP::MosTransposase + cc::gfp]) carrying the extrachromosomal Mostransposase under a heat-shock promoter was crossed into strain ttTi17821. 100 young adult worms (ttTi17821; nxEx166[HSP::MosTransposase + cc::gfp]) (P0) were heat-shocked (33°C; 1 h), allowed to recover for 1 h at 20°C, and heat-shocked again before removal to 20°C for 2 h. P0 worms were individually propagated and allowed to lay eggs (F1) for 24 h at 20°C. After removal of P0 worms, F1 worms were allowed to produce F2 progeny. DNA lysates from ∼50% of the F1–F2 worm mixture from each plate were prepared and PCR was performed using primers (5′-GCTACACGAAGACTAGTACTGTTC-3′ and 5′-GCGTTGATGAGAAGAACGAATG-3′) flanking the Mos insertion site. 100 worms from plates containing a *K07G5.3* deletion were cloned and screened for the deletion and homozygosed. Using this scheme, we isolated five *K07G5.3* alleles, including *nx105* (1828-bp deletion + 10-bp insertion; Fig. 3 A). Before analysis, *nx105* worms were outcrossed 5x to N2.

Imaging and subcellular localization of proteins

Live animals were anaesthetized using 10 mM levamisole (diluted in M9 buffer), mounted on 2% agar pads, and observed using epifluorescence or spinning-disc confocal microscopy performed on an inverted microscope (model 2000U; Nikon) outfitted with a spinning-disk laser apparatus (UltraVIEW ERS 6FE-US; PerkinElmer). Whole-mount immunostaining experiments were performed essentially as described previously (Bobinnec et al., 2000). In brief, gravid adults were cut in M9 buffer containing 15 mM levamisole to release gonads, intestine, and embryos. A coverslip was gently applied and the slide frozen in liquid nitrogen. The coverslip was then removed and the slide immersed in −20°C methanol for 5 min and air-dried for 5 min. Worms were rehydrated in PBS-BSA (1%) for 30 min, and incubated in 3% PBS-BSA with polyglutamylated tubulin antibody GT335 (1:2,500 dilution; a gift from Carsten Janke, Université Montpellier, Montpellier, France) for 1 h. After 3 × 10 min washes with PBS, anti–mouse secondary antibodies (Alexa 594; 1:1,000 dilution; Invitrogen) were applied in 3% PBS-BSA for 1 h. Slides were washed 3 × 10 min with PBS, mounted in ProLong gold (Invitrogen), and observed by confocal microscopy. All images were captured using OpenLab or Volocity (PerkinElmer).

Intraflagellar transport (IFT) assays

Anterograde IFT rate analyses were performed as described previously (Bialas et al., 2009; Inglis et al., 2009). Individual worms containing GFP-tagged IFT-associated proteins were picked onto 1% agar pads and immobilized using 10–20 mM levamisole. Amphid/phasmid cilia were examined with a 100x 1.35 NA objective and an ORCA AG CCD camera mounted on a Zeiss Axioskop 2 mot+ microscope. Images were acquired using Openlab version 5.0.2 (PerkinElmer), with exposure rates ranging from 150 ms/frame (for OSM-6::GFP–containing strains) to 250 ms/frame (for CHE-11::GFP–containing strains). Openlab LIFF files were imported, with relevant metadata, into ImageJ (http://rsb.info.nih.gov/ij/) using the

Bio-formats importer plug-in (Laboratory for Optical and Computational Instrumentation, University of Wisconsin-Madison, Madison, WI). Kymographs for IFT rate analyses were generated using the MultipleKymograph ImageJ plug-in (Inglis et al., 2009).

Phenotypic characterization

Ciliary analyses included dye-filling, lifespan, and osmotic avoidance assays.

Dye-filling assays. In brief, fluorescent dye uptake was performed as described previously (Jauregui et al., 2008). L4 larvae were incubated in Vybrant DiI (Invitrogen; 1:1,000-fold dilution of 1 mM stock in M9 buffer) for ~30 min, allowed to roam on a plate with bacteria for 1 h to clear intestinal dye, and observed by fluorescence microscopy.

Lifespan assays. Lifespan assays were performed exactly as described in Bialas et al. (2009). Each assay was performed twice with statistically significant results.

Osmosensation assays. Osmolarity avoidance assays were performed as described in Culotti and Russell (1978), testing for the crossing of worms over a ring of high osmolarity solution (8 M glycerol); 50 worms/strain were assayed, and experiments were repeated three times with statistically significant results.

UV sensitivity assays. The *mks-6(gk674)* deletion mutant removes a small portion of the *xpa-1* gene. We therefore tested if the *mks-6* mutant has lifespan and UV sensitivity phenotypes indicative of *xpa-1* dysfunction. Table S1 E reveals no lifespan defect for the *mks-6* mutant, and UV assays detailed below reveal no statistically significant increase in UV sensitivity of the *mks-6* mutant compared with wild-type. UV assays on *N2*, *mks-6(gk674)*, and *xpa-1(mn157)* worms were based on a protocol by Astin et al. (2008). Staged 1-d-old adults were placed onto NGM plates containing no food, then irradiated with a 254-nm UV Stratalinker 2400 (Agilent Technologies). 1 h after UV irradiation (100 J/m^2), worms were transferred to NGM plates containing OP50 bacteria and survival was scored thereafter every 24 h for 4 d. Each assay consisted of ~90 worms and was repeated three times.

Analysis of basal body, ciliary, and dendritic characteristics using IFT markers

Analyses of phasmid and amphid cilium lengths, dendrite lengths, and clustering of basal bodies was facilitated by visualizing the GFP-tagged IFT markers CHE-11 (IFT140) or OSM-6 (IFT52) in wild-type and mutant strains and quantitated using ImageJ; schematics depicting each of the four analyses are shown in Fig. 4, A–C; Fig. 5. In brief, ciliary axoneme lengths represent the distance between the distal end of the basal body and the tip of the cilium; dendrite lengths represent the distance between the beginning of a phasmid neuron cell body and its respective basal body; basal body clustering/distribution is the distance between the anterior-most and posterior-most basal bodies for each amphid channel. All measurements are repeated to statistical significance and reported in micrometers.

Transmission electron microscopy

Wild-type or mutant worms were washed directly into a primary fixative of 2.5% glutaraldehyde in 0.1M Sorensen phosphate buffer. To facilitate rapid ingress of fixative, worms were cut in half under a dissection microscope using a razor blade, transferred to Eppendorf tubes, and fixed for 1 h at room temperature. Samples were then centrifuged at 3,000 rpm for 2 min, supernatant removed and washed for 10 min in 0.1M Sorensen phosphate buffer. Worms were then post-fixed in 1% osmium tetroxide in 0.1M Sorensen phosphate buffer for 1 h at room temperature. After washing in buffer, specimens were processed for electron microscopy by standard methods; in brief, they were dehydrated in ascending grades of alcohol to 100%, infiltrated with epon, and placed in aluminum planchettes orientated in a longitudinal aspect and allowed to polymerize at 60°C for 24 h. Using a Leica UC6 ultramicrotome, individual worms were sectioned either in cross or longitudinal section, from anterior tip (for cross sections) or the side of the worm (for longitudinal sections), at 1 µm until the area of interest was located as judged by examining by light microscopy the sections stained with toluidine blue. Thereafter, serial ultra-thin sections of 80 nm were taken for electron microscopical examination. These were picked up onto 100 mesh copper grids and stained with uranyl acetate and lead citrate. Using a Tecnai Twin (FEI) electron microscope, sections were examined to locate, in the first instance, the most distal region of the ciliary region and subsequently from that point to the more proximal regions of the ciliary apparatus. At each strategic point, distal segment, middle segment, and transition zone/transition fiber regions were tilted using the Compustage of the Tecnai microscope to ensure that the axonemal microtubules were imaged in an exact geometrical normalcy to the imaging system. All images were recorded at an accelerating voltage (120 kV) and objective aperture of 10 µm using a MegaView 3 digital recording system.

HMM analyses and structural predictions of C2/B9 domains

HMMER profile hidden Markov model software suite (http://hmmer.janelia.org) was used to identify all C2 and B9 domains in the *C. elegans* genome and query their possible evolutionary relatedness. *C. elegans* C2 domains were first extracted from known *C. elegans* genes containing C2 domains (Table S1 C), and their alignment (obtained with ClustalW) was used as input for the HMMER program hmmbuild. Resulting profile was calibrated using hmmcalibrate and used to search the *C. elegans* proteome (version WS180) with hmmsearch. Using the same approach, we searched for B9 domain–containing genes in *C. elegans* using as input the three known B9 domains from MKS-1, MKSR-1, and MKSR-2 derived from three nematode species (*C. elegans*, *C. briggsae*, and *C. remanei*; Table S1 C). Structure predictions of the B9 domains from the human proteins MKS1, B9D1, and B9D2 were performed using the mGenTHREADER fold recognition program (McGuffin and Jones, 2003; http://bioinf.cs.ucl.ac.uk/psipred).

Online supplemental material

Table S1 (excel file) contains (A) conserved transition zone proteins and reported physical interactions, (B) *C. elegans* strains used in this study, (C) genome-wide HMM search for *C. elegans* proteins containing B9- and C2-related domains, (D) intraflagellar transport rate analyses for wild-type and TZ protein-disrupted strains, and (E) lifespan measurements. Figs. S1–S5 show ultrastructural (TEM) analysis of (S1) *mks-6;nphp-4*, (S2) *mks-5;nphp-4*, (S3) *mksr-1;nphp-4*, (S4) *mks-1;nphp-4*, and (S5) *mks-3;nphp-4* amphid channel cilia. Online supplemental material is available at http://www.jcb.org/cgi/content/full/jcb.201012116/DC1.

We thank N. Mahendran and N. Berbari for their assistance with the project, and the *C. elegans* gene knockout consortium, National Bioresource Project for *C. elegans*, and *Caenorhabditis* Genetics Center (CGC) for strains.

This work was funded by grants from the March of Dimes (to M.R. Leroux), Canadian Institutes of Health Research (CIHR; MOP-82870 to M.R. Leroux), Science Foundation Ireland (to O.E. Blacque), European Commission FP7 framework program (to O.E. Blacque), NIH P30 DK074038 Hepato/Renal Fibrocystic Diseases Core Center, NIH RO1 DK065655 (to B.K. Yoder), and NSERC (to N. Chen). C.L. Williams was supported by NIH T32 DK007545-22. P.N. Inglis was supported by a scholarship from MSFHR. N. Chen holds a scholar award from MSFHR and is a CIHR New Investigator. M.R. Leroux holds a senior scholar award from the Michael Smith Foundation for Health Research (MSFHR). O.E. Blacque is funded by the European Community's Seventh Framework Programme FP7/2009 under grant agreement no. 241955, SYSCILIA.

Submitted: 20 December 2010
Accepted: 17 February 2011

References

Astin, J.W., N.J. O'Neil, and P.E. Kuwabara. 2008. Nucleotide excision repair and the degradation of RNA pol II by the *Caenorhabditis elegans* XPA and Rsp5 orthologues, RAD-3 and WWP-1. *DNA Repair (Amst.)*. 7:267–280. doi:10.1016/j.dnarep.2007.10.004

Bae, Y.K., H. Qin, K.M. Knobel, J. Hu, J.L. Rosenbaum, and M.M. Barr. 2006. General and cell-type specific mechanisms target TRPP2/PKD-2 to cilia. *Development*. 133:3859–3870. doi:10.1242/dev.02555

Baker, K., and P.L. Beales. 2009. Making sense of cilia in disease: the human ciliopathies. *Am. J. Med. Genet. C. Semin. Med. Genet.* 151C:281–295. doi:10.1002/ajmg.c.30231

Beales, P.L., E. Bland, J.L. Tobin, C. Bacchelli, B. Tuysuz, J. Hill, S. Rix, C.G. Pearson, M. Kai, J. Hartley, et al. 2007. IFT80, which encodes a conserved intraflagellar transport protein, is mutated in Jeune asphyxiating thoracic dystrophy. *Nat. Genet.* 39:727–729. doi:10.1038/ng2038

Bialas, N.J., P.N. Inglis, C. Li, J.F. Robinson, J.D. Parker, M.P. Healey, E.E. Davis, C.D. Inglis, T. Toivonen, D.C. Cottell, et al. 2009. Functional interactions between the ciliopathy-associated Meckel syndrome 1 (MKS1) protein and two novel MKS1-related (MKSR) proteins. *J. Cell Sci.* 122:611–624. doi:10.1242/jcs.028621

Blacque, O.E., and M.R. Leroux. 2006. Bardet-Biedl syndrome: an emerging pathomechanism of intracellular transport. *Cell. Mol. Life Sci.* 63:2145–2161. doi:10.1007/s00018-006-6180-x

Blacque, O.E., M.J. Reardon, C. Li, J. McCarthy, M.R. Mahjoub, S.J. Ansley, J.L. Badano, A.K. Mah, P.L. Beales, W.S. Davidson, et al. 2004. Loss of *C. elegans* BBS-7 and BBS-8 protein function results in cilia defects

and compromised intraflagellar transport. *Genes Dev.* 18:1630–1642. doi:10.1101/gad.1194004

Blacque, O.E., E.A. Perens, K.A. Boroevich, P.N. Inglis, C. Li, A. Warner, J. Khattra, R.A. Holt, G. Ou, A.K. Mah, et al. 2005. Functional genomics of the cilium, a sensory organelle. *Curr. Biol.* 15:935–941. doi:10.1016/j.cub.2005.04.059

Bobinnec, Y., M. Fukuda, and E. Nishida. 2000. Identification and characterization of *Caenorhabditis elegans* gamma-tubulin in dividing cells and differentiated tissues. *J. Cell Sci.* 113:3747–3759.

Boulin, T., and J.L. Bessereau. 2007. Mos1-mediated insertional mutagenesis in *Caenorhabditis elegans*. *Nat. Protoc.* 2:1276–1287. doi:10.1038/nprot.2007.192

Brenner, S. 1974. The genetics of *Caenorhabditis elegans*. *Genetics*. 77:71–94.

Chapple, J.P., A.J. Hardcastle, C. Grayson, L.A. Spackman, K.R. Willison, and M.E. Cheetham. 2000. Mutations in the N-terminus of the X-linked retinitis pigmentosa protein RP2 interfere with the normal targeting of the protein to the plasma membrane. *Hum. Mol. Genet.* 9:1919–1926. doi:10.1093/hmg/9.13.1919

Craige, B., C.C. Tsao, D.R. Diener, Y. Hou, K.F. Lechtreck, J.L. Rosenbaum, and G.B. Witman. 2010. CEP290 tethers flagellar transition zone microtubules to the membrane and regulates flagellar protein content. *J. Cell Biol.* 190:927–940. doi:10.1083/jcb.201006105

Culotti, J.G., and R.L. Russell. 1978. Osmotic avoidance defective mutants of the nematode *Caenorhabditis elegans*. *Genetics*. 90:243–256.

Dammermann, A., H. Pemble, B.J. Mitchell, I. McLeod, J.R. Yates III, C. Kintner, A.B. Desai, and K. Oegema. 2009. The hydrolethalus syndrome protein HYLS-1 links core centriole structure to cilia formation. *Genes Dev.* 23:2046–2059. doi:10.1101/gad.1810409

Dawe, H.R., U.M. Smith, A.R. Cullinane, D. Gerrelli, P. Cox, J.L. Badano, S. Blair-Reid, N. Sriram, N. Katsanis, T. Attie-Bitach, et al. 2007. The Meckel-Gruber Syndrome proteins MKS1 and meckelin interact and are required for primary cilium formation. *Hum. Mol. Genet.* 16:173–186. doi:10.1093/hmg/ddl459

Deane, J.A., D.G. Cole, E.S. Seeley, D.R. Diener, and J.L. Rosenbaum. 2001. Localization of intraflagellar transport protein IFT52 identifies basal body transitional fibers as the docking site for IFT particles. *Curr. Biol.* 11:1586–1590. doi:10.1016/S0960-9822(01)00484-5

Dishinger, J.F., H.L. Kee, P.M. Jenkins, S. Fan, T.W. Hurd, J.W. Hammond, Y.N. Truong, B. Margolis, J.R. Martens, and K.J. Verhey. 2010. Ciliary entry of the kinesin-2 motor KIF17 is regulated by importin-beta2 and RanGTP. *Nat. Cell Biol.* 12:703–710. doi:10.1038/ncb2073

Fliegauf, M., T. Benzing, and H. Omran. 2007. When cilia go bad: cilia defects and ciliopathies. *Nat. Rev. Mol. Cell Biol.* 8:880–893. doi:10.1038/nrm2278

Gerdes, J.M., E.E. Davis, and N. Katsanis. 2009. The vertebrate primary cilium in development, homeostasis, and disease. *Cell*. 137:32–45. doi:10.1016/j.cell.2009.03.023

Gorden, N.T., H.H. Arts, M.A. Parisi, K.L. Coene, S.J. Letteboer, S.E. van Beersum, D.A. Mans, A. Hikida, M. Eckert, D. Knutzen, et al. 2008. CC2D2A is mutated in Joubert syndrome and interacts with the ciliopathy-associated basal body protein CEP290. *Am. J. Hum. Genet.* 83:559–571. doi:10.1016/j.ajhg.2008.10.002

Hao, L., and J.M. Scholey. 2009. Intraflagellar transport at a glance. *J. Cell Sci.* 122:889–892. doi:10.1242/jcs.023861

Hodges, M.E., N. Scheumann, B. Wickstead, J.A. Langdale, and K. Gull. 2010. Reconstructing the evolutionary history of the centriole from protein components. *J. Cell Sci.* 123:1407–1413. doi:10.1242/jcs.064873

Hoefele, J., R. Sudbrak, R. Reinhardt, S. Lehrack, S. Hennig, A. Imm, U. Muerb, B. Utsch, M. Attanasio, J.F. O'Toole, et al. 2005. Mutational analysis of the NPHP4 gene in 250 patients with nephronophthisis. *Hum. Mutat.* 25:411. doi:10.1002/humu.9326

Horst, C.J., L.V. Johnson, and J.C. Besharse. 1990. Transmembrane assemblage of the photoreceptor connecting cilium and motile cilium transition zone contain a common immunologic epitope. *Cell Motil. Cytoskeleton*. 17:329–344. doi:10.1002/cm.970170408

Hsiao, Y.C., Z.J. Tong, J.E. Westfall, J.G. Ault, P.S. Page-McCaw, and R.J. Ferland. 2009. Ahi1, whose human ortholog is mutated in Joubert syndrome, is required for Rab8a localization, ciliogenesis and vesicle trafficking. *Hum. Mol. Genet.* 18:3926–3941. doi:10.1093/hmg/ddp335

Inglis, P.N., O.E. Blacque, and M.R. Leroux. 2009. Functional genomics of intraflagellar transport-associated proteins in *C. elegans*. *Methods Cell Biol.* 93:267–304. doi:10.1016/S0091-679X(08)93014-4

Jauregui, A.R., K.C. Nguyen, D.H. Hall, and M.M. Barr. 2008. The *Caenorhabditis elegans* nephrocystins act as global modifiers of cilium structure. *J. Cell Biol.* 180:973–988. doi:10.1083/jcb.200707090

Jiang, S.T., Y.Y. Chiou, E. Wang, Y.L. Chien, H.H. Ho, F.J. Tsai, C.Y. Lin, S.P. Tsai, and H. Li. 2009. Essential role of nephrocystin in photoreceptor intraflagellar transport in mouse. *Hum. Mol. Genet.* 18:1566–1577. doi:10.1093/hmg/ddp068

Jin, H., S.R. White, T. Shida, S. Schulz, M. Aguiar, S.P. Gygi, J.F. Bazan, and M.V. Nachury. 2010. The conserved Bardet-Biedl syndrome proteins assemble a coat that traffics membrane proteins to cilia. *Cell*. 141:1208–1219. doi:10.1016/j.cell.2010.05.015

Keller, L.C., E.P. Romijn, I. Zamora, J.R. Yates III, and W.F. Marshall. 2005. Proteomic analysis of isolated *chlamydomonas* centrioles reveals orthologs of ciliary-disease genes. *Curr. Biol.* 15:1090–1098. doi:10.1016/j.cub.2005.05.024

Khanna, H., E.E. Davis, C.A. Murga-Zamalloa, A. Estrada-Cuzcano, I. Lopez, A.I. den Hollander, M.N. Zonneveld, M.I. Othman, N. Waseem, C.F. Chakarova, et al. 2009. A common allele in RPGRIP1L is a modifier of retinal degeneration in ciliopathies. *Nat. Genet.* 41:739–745. doi:10.1038/ng.366

Manandhar, G., P. Sutovsky, H.C. Joshi, T. Stearns, and G. Schatten. 1998. Centrosome reduction during mouse spermiogenesis. *Dev. Biol.* 203:424–434. doi:10.1006/dbio.1998.8947

McGuffin, L.J., and D.T. Jones. 2003. Improvement of the GenTHREADER method for genomic fold recognition. *Bioinformatics*. 19:874–881. doi:10.1093/bioinformatics/btg097

Moser, J.J., M.J. Fritzler, Y. Ou, and J.B. Rattner. 2010. The PCM-basal body/primary cilium coalition. *Semin. Cell Dev. Biol.* 21:148–155. doi:10.1016/j.semcdb.2009.06.006

Murcia, N.S., W.G. Richards, B.K. Yoder, M.L. Mucenski, J.R. Dunlap, and R.P. Woychik. 2000. The Oak Ridge Polycystic Kidney (orpk) disease gene is required for left-right axis determination. *Development*. 127:2347–2355.

Muresan, V., and J.C. Besharse. 1994. Complex intermolecular interactions maintain a stable linkage between the photoreceptor connecting cilium axoneme and plasma membrane. *Cell Motil. Cytoskeleton*. 28:213–230. doi:10.1002/cm.970280305

Nachury, M.V., A.V. Loktev, Q. Zhang, C.J. Westlake, J. Peränen, A. Merdes, D.C. Slusarski, R.H. Scheller, J.F. Bazan, V.C. Sheffield, and P.K. Jackson. 2007. A core complex of BBS proteins cooperates with the GTPase Rab8 to promote ciliary membrane biogenesis. *Cell*. 129:1201–1213. doi:10.1016/j.cell.2007.03.053

Nalefski, E.A., and J.J. Falke. 1996. The C2 domain calcium-binding motif: structural and functional diversity. *Protein Sci.* 5:2375–2390. doi:10.1002/pro.5560051201

Otto, E.A., B. Schermer, T. Obara, J.F. O'Toole, K.S. Hiller, A.M. Mueller, R.G. Ruf, J. Hoefele, F. Beekmann, D. Landau, et al. 2003. Mutations in INVS encoding inversin cause nephronophthisis type 2, linking renal cystic disease to the function of primary cilia and left-right axis determination. *Nat. Genet.* 34:413–420. doi:10.1038/ng1217

Ou, G., M. Koga, O.E. Blacque, T. Murayama, Y. Ohshima, J.C. Schafer, C. Li, B.K. Yoder, M.R. Leroux, and J.M. Scholey. 2007. Sensory ciliogenesis in *Caenorhabditis elegans*: assignment of IFT components into distinct modules based on transport and phenotypic profiles. *Mol. Biol. Cell*. 18:1554–1569. doi:10.1091/mbc.E06-09-0805

Perkins, L.A., E.M. Hedgecock, J.N. Thomson, and J.G. Culotti. 1986. Mutant sensory cilia in the nematode *Caenorhabditis elegans*. *Dev. Biol.* 117:456–487. doi:10.1016/0012-1606(86)90314-3

Roepman, R., S.J. Letteboer, H.H. Arts, S.E. van Beersum, X. Lu, E. Krieger, P.A. Ferreira, and F.P. Cremers. 2005. Interaction of nephrocystin-4 and RPGRIP1 is disrupted by nephronophthisis or Leber congenital amaurosis-associated mutations. *Proc. Natl. Acad. Sci. USA*. 102:18520–18525. doi:10.1073/pnas.0505774102

Rohatgi, R., and W.J. Snell. 2010. The ciliary membrane. *Curr. Opin. Cell Biol.* 22:541–546. doi:10.1016/j.ceb.2010.03.010

Rosenbaum, J.L., and G.B. Witman. 2002. Intraflagellar transport. *Nat. Rev. Mol. Cell Biol.* 3:813–825. doi:10.1038/nrm952

Satir, P., and S.T. Christensen. 2007. Overview of structure and function of mammalian cilia. *Annu. Rev. Physiol.* 69:377–400. doi:10.1146/annurev.physiol.69.040705.141236

Schwahn, U., S. Lenzner, J. Dong, S. Feil, B. Hinzmann, G. van Duijnhoven, R. Kirschner, M. Hemberger, A.A. Bergen, T. Rosenberg, et al. 1998. Positional cloning of the gene for X-linked retinitis pigmentosa 2. *Nat. Genet.* 19:327–332. doi:10.1038/1214

Sengupta, P., J.H. Chou, and C.I. Bargmann. 1996. odr-10 encodes a seven transmembrane domain olfactory receptor required for responses to the odorant diacetyl. *Cell*. 84:899–909. doi:10.1016/S0092-8674(00)81068-5

Sharma, N., N.F. Berbari, and B.K. Yoder. 2008. Ciliary dysfunction in developmental abnormalities and diseases. *Curr. Top. Dev. Biol.* 85:371–427. doi:10.1016/S0070-2153(08)00813-2

Shiba, D., D.K. Manning, H. Koga, D.R. Beier, and T. Yokoyama. 2010. Inv acts as a molecular anchor for Nphp3 and Nek8 in the proximal segment of primary cilia. *Cytoskeleton (Hoboken)*. 67:112–119.

Silverman, M.A., and M.R. Leroux. 2009. Intraflagellar transport and the generation of dynamic, structurally and functionally diverse cilia. *Trends Cell Biol.* 19:306–316. doi:10.1016/j.tcb.2009.04.002

Singla, V., M. Romaguera-Ros, J.M. Garcia-Verdugo, and J.F. Reiter. 2010. Ofd1, a human disease gene, regulates the length and distal structure of centrioles. *Dev. Cell*. 18:410–424. doi:10.1016/j.devcel.2009.12.022

Sorokin, S. 1962. Centrioles and the formation of rudimentary cilia by fibroblasts and smooth muscle cells. *J. Cell Biol.* 15:363–377. doi:10.1083/jcb.15.2.363

Sorokin, S.P. 1968. Centriole formation and ciliogenesis. *Aspen Emphysema Conf.* 11:213–216.

Stephan, A., S. Vaughan, M.K. Shaw, K. Gull, and P.G. McKean. 2007. An essential quality control mechanism at the eukaryotic basal body prior to intraflagellar transport. *Traffic*. 8:1323–1330. doi:10.1111/j.1600-0854.2007.00611.x

Tammachote, R., C.J. Hommerding, R.M. Sinders, C.A. Miller, P.G. Czarnecki, A.C. Leightner, J.L. Salisbury, C.J. Ward, V.E. Torres, V.H. Gattone II, and P.C. Harris. 2009. Ciliary and centrosomal defects associated with mutation and depletion of the Meckel syndrome genes MKS1 and MKS3. *Hum. Mol. Genet.* 18:3311–3323. doi:10.1093/hmg/ddp272

Tory, K., T. Lacoste, L. Burglen, V. Morinière, N. Boddaert, M.A. Macher, B. Llanas, H. Nivet, A. Bensman, P. Niaudet, et al. 2007. High NPHP1 and NPHP6 mutation rate in patients with Joubert syndrome and nephronophthisis: potential epistatic effect of NPHP6 and AHI1 mutations in patients with NPHP1 mutations. *J. Am. Soc. Nephrol.* 18:1566–1575. doi:10.1681/ASN.2006101164

Williams, C.L., M.E. Winkelbauer, J.C. Schafer, E.J. Michaud, and B.K. Yoder. 2008. Functional redundancy of the B9 proteins and nephrocystins in *Caenorhabditis elegans* ciliogenesis. *Mol. Biol. Cell*. 19:2154–2168. doi:10.1091/mbc.E07-10-1070

Williams, C.L., S.V. Masyukova, and B.K. Yoder. 2010. Normal ciliogenesis requires synergy between the cystic kidney disease genes MKS-3 and NPHP-4. *J. Am. Soc. Nephrol.* 21:782–793. doi:10.1681/ASN.2009060597

Winkelbauer, M.E., J.C. Schafer, C.J. Haycraft, P. Swoboda, and B.K. Yoder. 2005. The *C. elegans* homologs of nephrocystin-1 and nephrocystin-4 are cilia transition zone proteins involved in chemosensory perception. *J. Cell Sci.* 118:5575–5587. doi:10.1242/jcs.02665

Yin, Y., F. Bangs, I.R. Paton, A. Prescott, J. James, M.G. Davey, P. Whitley, G. Genikhovich, U. Technau, D.W. Burt, and C. Tickle. 2009. The Talpid3 gene (KIAA0586) encodes a centrosomal protein that is essential for primary cilia formation. *Development*. 136:655–664. doi:10.1242/dev.028464

Zaghloul, N.A., and N. Katsanis. 2010. Functional modules, mutational load and human genetic disease. *Trends Genet.* 26:168–176. doi:10.1016/j.tig.2010.01.006